

Article

Evaluation of a Novel High-Efficiency SHS-EAH Multi-Stage DG-ADP Process for Cleaner Production of High-Quality Ferrovandium Alloy

Bin Yu ^{1,2}, Tiechui Yuan ^{1,*}, Junjie Shi ^{3,4,*}, Ruidi Li ¹, Chenglong Jiang ^{3,4}, Mingfeng Ye ², Daihong Xiao ¹ , Haijun Chen ², Lin Zhang ⁵, Ning Wang ², Leizhang Gao ², Danfeng Yin ², Lei Zhang ² and Xiong Yang ⁵

¹ Powder Metallurgy Research Institute, Central South University, Changsha 410012, China; robinyjgc@sina.com (B.Y.); liruidi@csu.edu.cn (R.L.); daihongx@csu.edu.cn (D.X.)

² State Key Laboratory of V and Ti Resources Comprehensive Utilization, Ansteel Research Institute of Vanadium & Titanium (Iron & Steele), Panzhihua 617000, China; csuymf@163.com (M.Y.); chjnavy@126.com (H.C.); 13840512392@163.com (N.W.); gaoleizhang2016@163.com (L.G.); danfengyin2013@163.com (D.Y.); zhangleiwood@163.com (L.Z.)

³ Key Laboratory for Ecological Metallurgy of Multimetallc Mineral (Ministry of Education), Northeastern University, Shenyang 110819, China; 15886153906@163.com

⁴ School of Metallurgy, Northeastern University, Shenyang 110819, China

⁵ Pangang Group Vanadium & Titanium Resources Co., Ltd., Panzhihua 617000, China; gcmmlin@163.com (L.Z.); 15183431320@163.com (X.Y.)

* Correspondence: tiechuiyuan@csu.edu.cn (T.Y.); junjieshi@126.com (J.S.)

Abstract: A novel high-efficiency industrialized clean production technology based on multi-stage gradient batching and smelting was proposed for the production of high-quality ferrovanadium. The thermodynamic mechanism of aluminothermic reduction equilibrium, alloy settlement and raw material impurity distribution were confirmed, and a multi-stage double-gradient aluminum addition pattern (DG-ADP), the highly efficient separation of molten slag and alloy, and typical impurity control standards of raw materials were achieved on the basis of a self-propagating high-temperature synthesis with an electric auxiliary heating (SHS-EAH) process. The reduction efficiency, separation efficiency and the comprehensive utilization rate of the secondary resources were significantly improved, as the whole total vanadium (T.V) content in the industrially produced residue slag reduced from 2.34 wt.% to 0.60 wt.%, while the corresponding smelting yield increased from 93.7 wt.% to 98.7 wt.% and the aluminum consumption decreased from 510 kg·t⁻¹ to 400 kg·t⁻¹. The multi-stage DG-ADP process enabled the internal circulation of vanadium-bearing materials in the ferrovanadium smelting system, as well as the external circulation of iron and residue slag in the same system, and finally achieved the zero discharge of solid and liquid waste from the ferrovanadium production line, which provides a brand-new perspective for the cleaner production of ferrovanadium alloy.

Keywords: ferrovanadium; aluminothermic; separation; inclusions; multi-stage; gradient batching



Citation: Yu, B.; Yuan, T.; Shi, J.; Li, R.; Jiang, C.; Ye, M.; Xiao, D.; Chen, H.; Zhang, L.; Wang, N.; et al. Evaluation of a Novel High-Efficiency SHS-EAH Multi-Stage DG-ADP Process for Cleaner Production of High-Quality Ferrovandium Alloy. *Metals* **2024**, *14*, 211. <https://doi.org/10.3390/met14020211>

Academic Editor: Petros E. Tsakiridis

Received: 7 January 2024

Revised: 24 January 2024

Accepted: 2 February 2024

Published: 8 February 2024



Copyright: © 2024 by the authors. Licensee MDPI, Basel, Switzerland. This article is an open access article distributed under the terms and conditions of the Creative Commons Attribution (CC BY) license (<https://creativecommons.org/licenses/by/4.0/>).

1. Introduction

Vanadium has been regarded as an important strategic alloying element, and is known as industrial monosodium glutamate [1,2]. It is a crucial nonferrous metal and a strategic material extensively applied in steelmaking, chemical, aerospace and defense and alloy preparation. Major market-oriented vanadium products including vanadium oxides (e.g., V₂O₃, V₂O₅) and V-based intermediate alloys (e.g., FeV, AlV, VN) are widely used in the iron and steel industry, catalysis, certain alloys and vanadium electrolytes and the pigments and material industries [3–6]. Other vanadium products with broad applications are mainly used in high-purity sputtering targets, functional films, radio resistance barriers and other functional fields. Therefore, it is of great importance to increase the productivity of vanadium-based production to meet the huge demand of the future of this market.

Vanadium-bearing slag is the most important secondary source, which is a by-product generated in the semi-steel producing and vanadium removal step in the steel-making process using vanadium-rich titanomagnetite ore as the raw material [7,8]. In vanadium-bearing minerals, vanadium in minerals is found in the form of vanadates or oxides, forming spinel group solid solutions together with iron, titanium, chromium or manganese [9,10]. Over the past 20 years, vanadium-bearing slags have mainly been treated using the sodium salt roast-leaching process or calcium salt roast-leaching process for the extraction of vanadium [11,12]. A high temperature and strong oxidation atmosphere are employed to facilitate the dissolution of vanadium [13–15]. Due to the environmental restrictions of the traditional roast-leaching process and the rapid development of hydrometallurgical leaching technology, the blank roasting, composite roasting and direct acid leaching processes for vanadium extraction have also been receiving considerable attention to improve the efficiency, yield and comprehensive resource utilization [16–19]. Through the above processes, a high quality and high yield of vanadium oxides are obtained to meet the feedstock requirements of back-end products.

More than 90% of produced vanadium is added into steel as an intermediate alloy in the form of ferrovanadium (e.g., FeV50, FeV60, FeV80), which is mainly prepared by the self-propagating high-temperature synthesis (SHS) process with a mixture composed of vanadium oxides, reducing agents and fluxing agents [20]. The SHS process is also known as combustion synthesis and involves combustion modes and thermal explosion modes through chemical reactions, which are widely applied to the preparation of master compounds and alloys [21–24]. The SHS technology is propelled by the heat release from chemical reactions completely or partially, and nearly no external heat sources are needed. Products with desired components and structures are obtained by a self-sustaining reaction of rapid automatic wave combustion. The speed, temperature and conversion rate of SHS are mainly determined by the heat release and transfer rate.

Aluminum (Al) and Silicon (Si) are the most widely used reducing agents for SHS reactions [25–27]. Compared with silicothermic reduction, the aluminothermic reduction process has the advantages of being a shorter process, allowing greater heat release and lower environmental risks, and therefore has become the most widely used engineering process for the industrial preparation of ferrovanadium [28]. Over the past few decades, the aluminothermic process has been widely used as the main technology by Pangang Group Co., Ltd. (Panjihua, China), HBIS Group Co., Ltd. (Shijiazhuang, China), Evraz (Moscow, Russia), etc. Nowadays, with the gradual maturity of high-temperature metallurgical equipment technology and the rapid increase in the demand of the ferrovanadium market, the smelting of ferrovanadium has gradually evolved from a one-step reduction in small straight tube furnaces to two-step reductions or even multi-stage reductions in large tilting electric furnaces [29,30]. However, the industrial residue vanadium in slag cannot be reduced to the theoretical reduction limit, regardless of what kinds of processes or equipment are used, leading to the rising of the cost and waste of high-value resources. The disparity between the amount of reduction agent added and the product composition (aluminum content) cannot be fundamentally reconciled, and the properties of the smelting slag from aluminothermic reduction also leads to the difficult separation of slag and alloy. How to solve the above problems has become an urgent industrial issue for the production of high-quality ferrovanadium alloy [31].

In order to solve the general technical problems and enhance the whole vanadium yield, a high-efficiency industrialized clean process for the production of ferrovanadium from vanadium oxides was proposed. In this study, different reaction principles were selected from the perspective of thermodynamic equilibrium between the coexisting slag and target alloy. Furthermore, an improved self-propagating high-temperature synthesis with electric auxiliary heating (SHS-EAH) process was designed to synthesize ferrovanadium based on a multi-stage gradient aluminum addition pattern (MS-G-ADP), and the influence of the two different reduction processes on the quality of the ferrovanadium was compared. All the process parameters were optimized, and the mechanisms of reduction,

sedimentation and impurity control were proved, which can provide significant guidance for the industrial preparation of ferrovandium.

2. Experimental Procedure

2.1. Materials and Apparatus

The auxiliary materials supplied from Pangang Group including vanadium source, iron source, reduction agent and fluxing medium are listed in Table 1, which are consistent with the national standard of China (GB/T), industrial standard of the Chinese Society of Metals (YB/T) or company standard of Pangang Group, (QB). The total vanadium (T.V) mass content of vanadium-bearing secondary resources such as fly ash, collected dust and vanadium-rich smelting slag (VRSS) are higher than 10.0 wt.%, 15.0 wt.% and 3.0 wt.%, respectively. The remaining components of the above vanadium-bearing secondary resources are mainly oxides of highly reducing metals, such as Al_2O_3 , MgO and CaO. The fluxing medium has a particle size ranging from 20 to 50 mm and contains more than 90.0 wt.% CaO. The iron source, which can be either scrap iron or ball-milled iron granules (BMIG), has dimensions of 5 to 10 mm in length and 3.0 to 5.0 mm in width. The reducing agent possesses a particle size between 1.0 and 5.0 mm and contains over 99.0 wt.% aluminum.

Table 1. Typical chemical composition and requirements of the auxiliary materials.

Original Materials	Purity, \geq wt. %	Impurities Limitation, \leq wt. %					Standards	
		Si	Mn	C	P	S		
Vanadium sources	V_2O_3	62.0 (T.V)	0.08	--	0.10	0.02	0.06	GB/T 40301–2021 [32]
	V_2O_5	98.0	0.11	--	0.04	0.05	0.03	YB/T 5304–2017 [33]
	FeV	48.0 (T.V)	1.50	0.50	0.30	0.08	0.06	GB/T 4139-2012 [34]
	Fly ash	10.0 (T.V)	2.00	0.50	0.50	0.10	0.10	
	Collected dust	15.0 (T.V)	2.00	0.06	0.50	0.10	0.10	
	VRSS	3.0 (T.V)	1.50	0.06	0.30	0.10	0.10	
Iron sources	Scrap iron	99.0	0.10	0.10	0.10	0.05	0.05	QB–2021 [35]
	BMIG	95.0	0.25	0.20	0.10	0.05	0.05	
Reduction agent	Al	99.0	0.05	0.05	0.10	0.05	0.05	
Fluxing medium	CaO	90.0	0.10	0.05	0.10	0.05	0.05	

An enhanced SHS-EAH process was implemented in a tilting furnace equipped with multiple slag and alloy discharge capabilities, as depicted in Figure 1. The tilting furnace consists of four main systems: loading, heating, cooling and discharge. The loading system features stock bins for each batch of mixed ingredients and fluxing agent, a slag pan for residue slag, and an ingot mold for alloy and remaining slag, with capacities of approximately 30.0 t, 10.0 t and 15.0 t, respectively. The heating system employs a three-phase electrode with a rated capacity of 6300 kVA and a three-stage voltage regulation of 150 V, 170 V and 190 V, designed to initiate the SHS-EAH reaction and maintain the temperature of the system. The cooling system primarily comprises a water-cooling roof and a water-cooling wall. The discharge system includes a slag hole for the discharge of molten slag and a tap hole for the casting of molten slag and alloy.

2.2. Framework and Methods

The structure of the enhanced industrial SHS-EAH process for ferrovandium production using MS-G-ADP is illustrated in Figure 2. Key process parameters tied to essential technical metrics, such as smelting yield, efficiency, secondary resource utilization, and product quality, were comprehensively investigated. Theoretical studies on reduction thermodynamics, infinite fluid gravity sedimentation, impurity management and removal were based on reaction equilibrium, phase diagrams, Stokes' law of settling and slag properties. Results and their analyses, along with countermeasures, are discussed. Additionally, an evaluation of the efficient and clean industrial production of ferrovandium is presented.

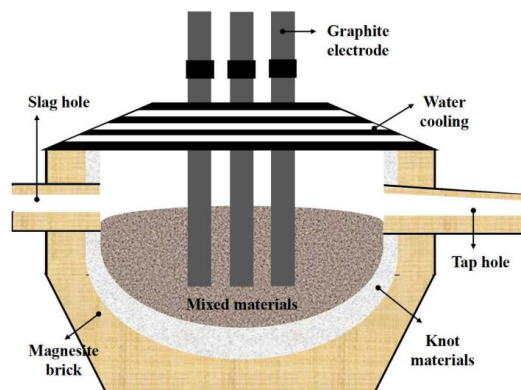


Figure 1. Schematic diagram of the tilting furnace for SHS-EAH process.

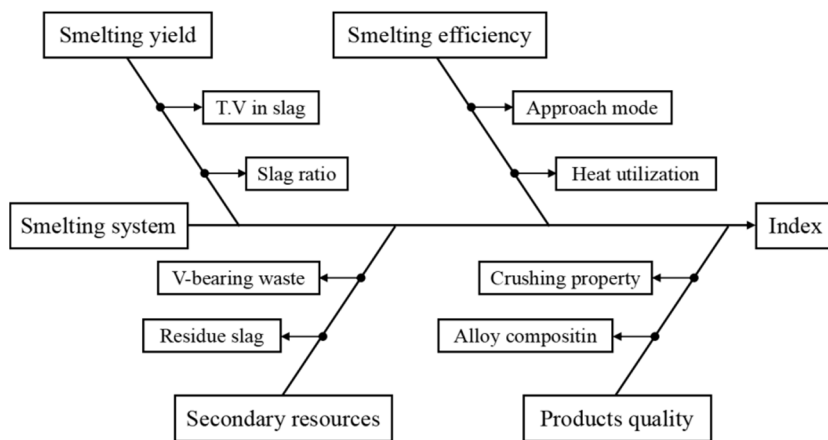


Figure 2. Conceptual framework of industrialized process for ferrovanadium preparation by MS-G-ADP.

The industrialized SHS-EAH process for ferrovanadium preparation by MS-G-ADP is presented in Figure 3. The raw materials were accurately weighted with the pre-calculated mass ratios according to different smelting periods and different smelting batches, and then thoroughly ground and mixed for at least 10 min in an industrial blending system. The mixed materials were transported to the smelting area and placed into the stoke bin for feeding and smelting in stages. Multiple feeding and discharging were adopted based on different ingredient principles during the smelting process. More than 80.0 wt.% of the molten slag produced in each smelting stage were discharged through a slag hole, and all the molten alloy and residual slag in the last smelting stage were cast into the ingot mold through a tap hole. After splitting the casting ingot mold, the alloy ingot and the high-alumina-content corundum slag were obtained, respectively. The alloy ingot with qualified composition was divided and shipped after crushing, while the sub-quality product was returned to the bottom of tilting furnace for remelting. The waste corundum slag was totally broken and used for the preparation of refractory material or slag-making material in steel industry.

In order to achieve the efficient utilization of waste in the whole process, the systematically produced and collected vanadium-bearing secondary resources, such as precipitator ash, enriched dust and vanadium-rich residue slag, were pelleted and dried for secondary smelting. In order to achieve the low-cost smelting of raw materials, the traditional high-price scrap iron was replaced by BMIG, which was obtained by magnetic separation of coarse vanadium slag in the front operation. Through the above technological measures, the on-line circulation of waste materials and the demand of low-cost raw material smelting were intended to be established.

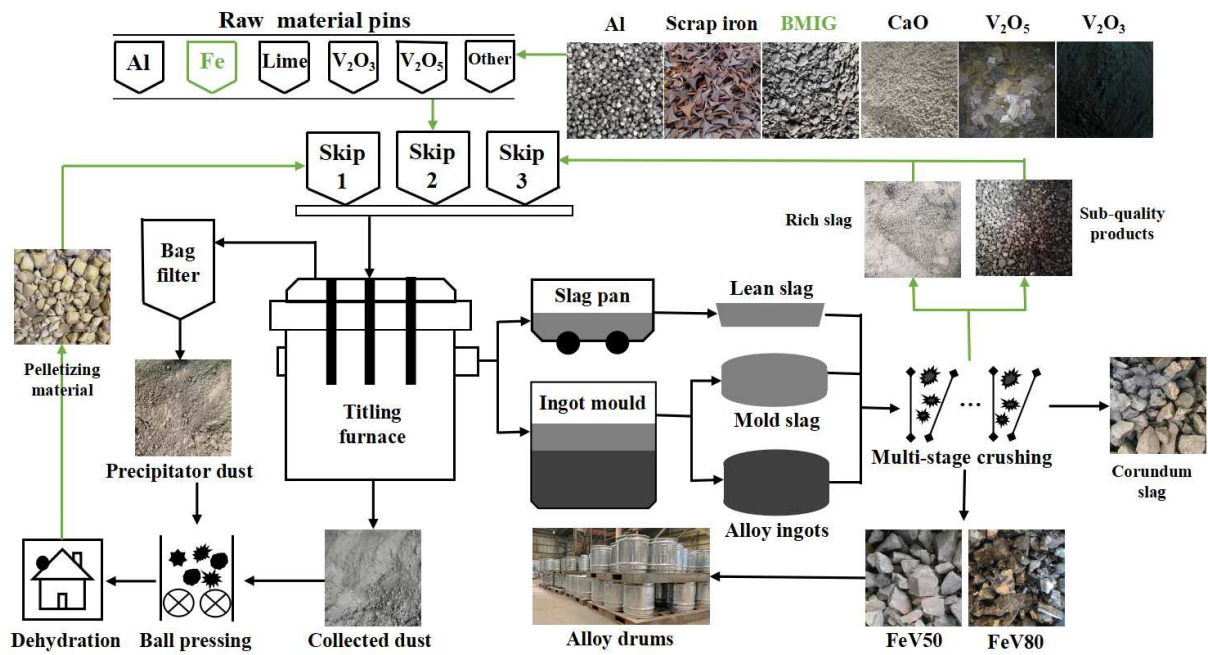


Figure 3. Process flow chart of ferrovanadium smelting on-line circulation.

According to the experimental design scheme shown in Figure 4, the key step is the addition and smelting of mixed raw materials in the tilting furnace. Taking 3-stage smelting as an example, feeding, smelting, separation discharging and casting are the necessary processes for each stage. The 1st stage and 2nd stage involves feeding, smelting, separation and tilting, while the 3rd stage involves feeding, smelting, separation and casting. Feeding process of each smelting stage is divided into two batches with the change in the aluminum coefficient.

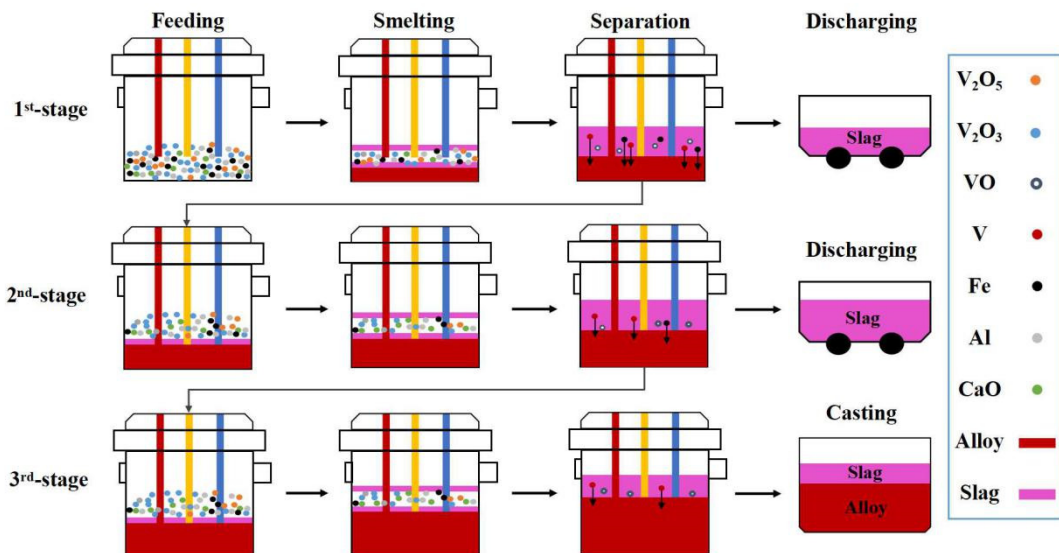


Figure 4. Three-stage smelting process diagram.

In the multi-stage smelting process, the dosage of theoretical aluminum addition at each stage can be determined using various modes: uniform, semi-gradient, single-gradient and double-gradient, while keeping the comprehensive aluminum coefficient essentially constant. In the uniform aluminum distribution pattern (U-ADP), akin to the one-step smelting process in reference [36], there is a consistent aluminum addition coefficient across all stages. In contrast, the multi-stage gradient aluminum distribution patterns exhibit

varying aluminum addition coefficients at each stage. For instance, the semi-gradient aluminum distribution pattern (SeG-ADP) is characterized by the addition of an excessive amount of reducing agent in the 1st and 2nd stages, with no reducing agent added in the 3rd stage. The single-gradient aluminum distribution pattern (SiG-ADP) is structured with a decreasing aluminum addition coefficient from one stage to the next. Meanwhile, the double-gradient aluminum distribution pattern (DG-ADP) not only decreases the aluminum addition coefficient between each stage but also increases it between two batches within each stage.

Specifically, the main parameter involved in the experimental process mainly includes aluminum distribution pattern, separation of molten slag and alloy and standards for impurity components of raw materials. The aluminum distribution coefficient (η) range from 0 to 1.5 in different smelting stages along with the aluminum distribution rules of increasing in periods and decreasing between periods. The slag thickness ranges from 30 cm to 55 cm, casting temperature ranges from 1830 °C to 1950 °C and insulation thickness ranges from 0 to 15 cm during the casting and separation process. And the characteristics of slag varies with the change of corresponding typical composition of molten slag.

2.3. Characteristics

Before smelting, precise mixing models for different batches of original materials in each smelting stage were established. The consumption of aluminum (M_{Al}) and iron (M_{Fe}) is shown in Equations (1) and (2) as follows, respectively:

$$M_{Al} = \sum_i^n (M_i m_i \eta) \div w_{Al} \quad (1)$$

$$M_{Fe} = \sum_i^n (M_i w_{Vi}) \times Y_S \div r_{V/Fe} \quad (2)$$

where M_i and m_i are the input mass content and aluminum consumption of different vanadium resources with units of kg; η is the composite aluminum addition coefficient; w_{Al} and w_{Vi} are the purity of aluminum and different vanadium resources with units of wt.%, respectively; Y_S is the smelting yield of vanadium (%); $r_{V/Fe}$ is the mass ratio of vanadium and iron with units of $\text{kg} \cdot \text{kg}^{-1}$. The actual dosage aluminum and iron is mainly affected by the type, purity, weight and mixing coefficient of different raw materials. The aluminum consumption of V_2O_3 , V_2O_5 and other vanadium-bearing secondary resources and weak reducing metals or non-metallic oxides are calculated based on oxygen balance, vanadium balance and theoretical aluminum dosage, respectively. The iron dosage is mainly affected by the type of iron source. Non-standard vanadium source and iron source were pre-treatment by crushing and screening, and then mixed with other standard raw materials. The smelting yield (Y_S) and comprehensive yield (Y_C) of vanadium used to quantify this technical indicator of the above process is expressed according to Equations (3) and (4), as follows, respectively:

$$Y_S = \left(1 - \frac{w_{V-S} R_{S/A}}{w_{V-A}} \right) \times 100\% \quad (3)$$

$$Y_C = \left(1 - \frac{\sum_{O=1}^2 M_O V_O}{\sum_I^N M_I V_I} \right) \div w_{V-A} \times 100\% \quad (4)$$

where w_{V-S} and w_{V-A} are the mass content of vanadium in residue slag and alloy, respectively, with units of wt.%; $R_{S/A}$ is the mass ratio of slag and alloy with units of $\text{kg} \cdot \text{kg}^{-1}$; M_O and V_O are the output product mass of alloy and mass content of vanadium in smelting residue, respectively; M_I and V_I are the input mass and mass content of vanadium in original vanadium source, respectively, with units of kg. The criterion for the reaction endpoint is mainly based on the standard of T.V in slag decreasing less than 0.1% per 10 min.

FactSage[®] 8.3 software was adopted to predict the slag characteristics and reactions during the smelting process. The "Equili", "Viscosity" and "Phase diagram" module was used to investigate the reaction feasibility, slag viscosity and melting point, and phase

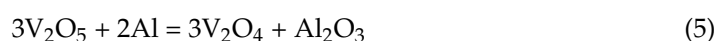
equilibrium. The phase assemblies of the solid samples were identified via X-ray diffraction analysis (XRD, D8-advance, Bruker, Birica, MA, USA) using Co K α radiation at a scan rate of 5 $^{\circ}$ ·min $^{-1}$ from 10 $^{\circ}$ to 100 $^{\circ}$ with an acceleration voltage of 40 kV and current of 40 mA. The chemical compositions of raw materials, products, by-products and residue slag were analyzed using X-ray fluorescence (XRF, Simultix14, RC, Tokyo, Japan) at scan angle from 50 $^{\circ}$ to 150 $^{\circ}$ with a measuring voltage of 50 kV and current of 60 mA. The apparent morphologies and element distribution in different phases were observed by means of field emission scanning electron microscopy and an energy-dispersive X-ray spectrometer (SEM-EDS, ULTRA PLUS, ZEISS, Tokyo, Japan) with a voltage of 20 kV, collection time of 20 ms and electron beam working distance of 10 mm. The phase compositions and mineral structure were analyzed using the image processing software of mineral liberation analyzer (MLA, Quanta650, Houston, TX, USA) based on the analysis results of SEM-EDS.

3. Results and Discussion

3.1. Thermodynamic Principle of Aluminothermic Reduction

3.1.1. Thermodynamic Equilibrium of V-Al-O

According to the principle of step-by-step reduction, the SHS reaction of vanadium oxides by aluminothermic reduction are gradually reduced from a high valence state to a low valence state, V₂O₅ can be reduced to V₂O₄, V₂O₃, VO and even to metal with the increase in temperature and Al addition, as illustrated by reactions (5) to (8) [37], and the Gibbs free energy (ΔG^{\ominus}) for aluminothermic reduction of different vanadium oxides are presented in Figure 5. The un-reduced vanadium with an occurrence state of V₂O₃ or VO in molten slag is related to the content of the reduced product V and reducing agent Al [38]. When slag and alloy coexist in a smelting system, a large amount of reduced metal vanadium can form in the molten alloy phase through the equilibrium reaction between low-valence V₂O₃ and VO and Al, as shown in reaction (9). The corresponding ΔG^{\ominus} for reaction (9) was calculated to be $-85.0 \text{ kJ}\cdot\text{mol}^{-1}$ at 1800 $^{\circ}\text{C}$, which means that VO is more thermodynamically stable than V₂O₃. On the other hand, when slag and alloy are separated completely after smelting, VO in molten slag may be oxidized again. According to reaction (10), the relative stability of VO and V₂O₃ is related to the system temperature and ambient oxygen partial pressure. The equilibrium oxygen partial pressure is calculated to be 0.41 Pa at 1800 $^{\circ}\text{C}$, while the actual oxygen partial pressure during operation is much higher than the equilibrium oxygen partial pressure, and VO will be oxidized to be V₂O₃.



Based on the thermodynamic analysis, the reaction mechanism of aluminothermic reduction for vanadium alloy is deduced, as presented in Figure 6. High-valence vanadium oxides are reduced into vanadium metal step by step, and the produced vanadium metal is combined with iron to form metal-bonded compounds during settlement. The main restrictive step is the transmission of vanadium oxides from the molten slag to the reaction interface, where the vanadium oxide is continuously reduced by aluminum at the slag–alloy interface.

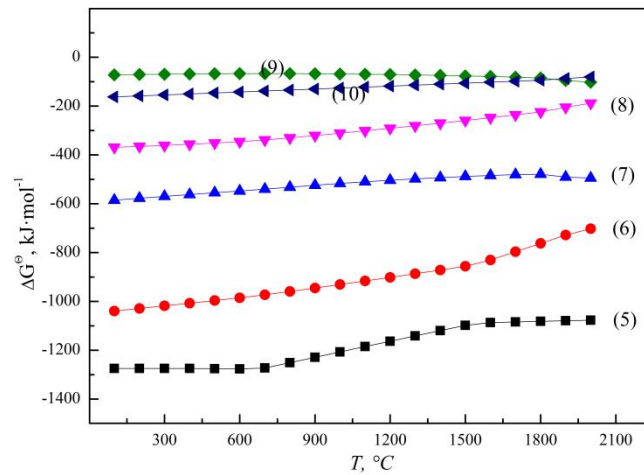


Figure 5. ΔG^\ominus for aluminothermic reduction of different vanadium oxides.

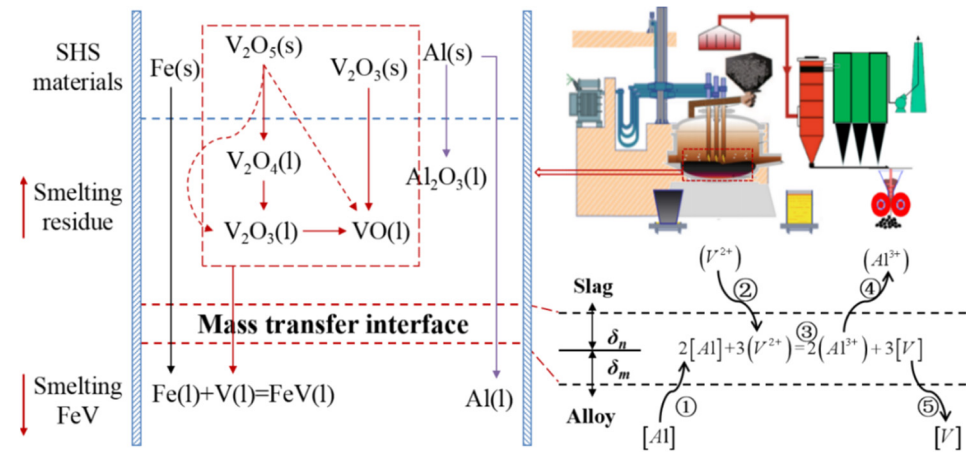


Figure 6. Mechanism of aluminothermic reduction for ferrovanadium.

The direction and limitation of chemical reactions can be determined by the Van't Hoff isothermal equation; the influencing factors include the reaction temperature and the generalized activity ratio [39]. The generalized activity ratio (J) gradually stabilizes to the reaction equilibrium constant (K) when the reaction reaches equilibrium. According to the thermodynamic equilibrium of V-Al-O, the slag–alloy equilibrium of ferrovanadium is controlled by reaction (8) in the case of sufficient amounts of the aluminum reducing agent. The relationship between the products and reactants can be expressed as Equations (11) and (12) from the definition of the equilibrium constant of the chemical reactions.

$$\Delta G^\ominus = -RT \ln \frac{a_{[V]}^3 \cdot a_{(Al_2O_3)}}{a_{(VO)}^3 \cdot a_{[Al]}^2} \quad (11)$$

$$\ln N_{(VO)} = \frac{\Delta G^\ominus}{3RT} - \frac{\ln r_{(VO)}^3 \cdot r_{[Al]}^2}{3} + \frac{\ln a_{[V]}^3 \cdot a_{(Al_2O_3)}}{3} - \frac{2 \ln N_{[Al]}}{3} \quad (12)$$

where ΔG^\ominus is the standard *Gibbs* free energy of reaction (8), $J \cdot mol^{-1}$; R is the gas constant, $8.314 J \cdot mol^{-1} \cdot K^{-1}$. T is temperature, K ; N , a and r are the molar percentage, activities and activities coefficient of each substance, %, respectively. Due to the fact that V and Al_2O_3 are the dominant metallic phase and slag phase, the activity of V and Al_2O_3 are approximately equal to 1.0. In the absence of the thermodynamic data of the activity coefficient, the activity of VO in slag and Al in alloy can approximately be replaced by molar fraction N_{VO} and N_{Al} , which means the activity coefficient of VO and Al are also approximated as the constant 1.

Therefore, the relationship between the activity of VO in the slag and the activity of Al in the alloy can be simplified and is presented as Equation (13) to Equation (15).

$$N_{(\text{VO})} = e^{\Delta G^\ominus / 3RT} \div \left(N_{[\text{Al}]} \right)^{2/3} \quad (13)$$

$$N_{(\text{VO})} = \frac{M_{(\text{Al}_2\text{O}_3)} \cdot w_{(\text{VO})}}{(M_{(\text{VO})} + w_{(\text{VO})} \cdot M_{(\text{Al}_2\text{O}_3)} - w_{(\text{VO})} \cdot M_{(\text{VO})}) \cdot w_{(\text{Al}_2\text{O}_3)} \cdot r_{\text{slag}}} \times 100\% \quad (14)$$

$$N_{[\text{Al}]} = \frac{M_{[\text{V}]} \cdot w_{[\text{Al}]}}{(M_{[\text{Al}]} + w_{[\text{Al}]} \cdot M_{[\text{V}]} - w_{[\text{Al}]} \cdot M_{[\text{Al}]}) \cdot w_{[\text{V}]}} \times 100\% \quad (15)$$

where $M_{\text{Al}_2\text{O}_3}$, M_{VO} , M_{Al} and M_{V} are the molar masses of Al_2O_3 , VO, Al and V, respectively. $w_{\text{Al}_2\text{O}_3}$, w_{VO} , w_{Al} and w_{V} are the mass fraction of Al_2O_3 , VO in the slag and Al and V in the alloy, respectively, wt.%. r_{slag} is the mass ratio of the actual slag in the furnace to the theoretical total slag, %. According to Equations (13)–(15), the reduction limitation of reaction (8) is mainly affected by the standard Gibbs free energy, aluminum addition coefficient, slag–alloy mass ratio and different alloy grades. The relationship between the VO content in the slag and the Al content in the alloy at different temperatures was calculated as shown in Figure 7. The calculated results indicate the great influence of the Al content on the VO content, which provides theoretical guidance for the experimental aluminothermic reduction. For example, the theoretical VO content in the slag decreases from 3.55 wt.% to 0.64 wt.% with the increase in the aluminum content from 0.2 wt.% to 2.5 wt.% in FeV50 at 1700 °C. With the further increase in the Al content to 20.0 wt.%, the theoretical VO content and the corresponding T.V in the slag decreases to 0.16 wt.% and 0.12 wt.%, respectively. In order to effectively control the vanadium loss in the slag and reduce the VO content to less than 0.2 wt.%, the corresponding Al content in the alloy should be higher than 14.0 wt.%, which means a great excess of Al should be added to promote a deep reduction.

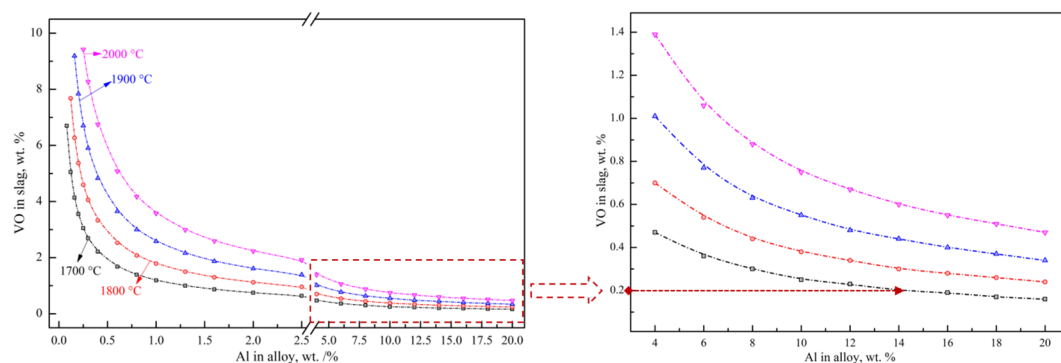


Figure 7. Relations between Al in alloy and VO in slag.

3.1.2. Multi-Stage Gradient Addition for Aluminothermic Reduction

In order to verify the calculated thermodynamic trend, a validation experiment was designed to investigate the effect of the aluminum addition coefficient on the T.V (total vanadium) in the slag for a comprehensive comparison with a different aluminum addition pattern, with the premise of Al in the alloy not exceeding the standard of 2.5 wt.%. Based on the results of the thermodynamic equilibrium of V-Al-O, the three-stage SHS-EAH process of the gradient aluminum addition pattern was carried out. The discharged slag of each stage was controlled at 80 wt.% of the theoretical slag, and the unit power supply was controlled at about $550 \text{ kVA} \cdot \text{t}^{-1}$ to meet the melting temperature range from 1800 °C to 2000 °C. The different feeding modes and aluminum distribution coefficient were designed in Table 2 and Figure 8, and the corresponding T.V in the molten slag and conducting time were expressed in Figure 9. The reduction of vanadium is effectively promoted by

improving the aluminum addition coefficient. When the aluminum distribution coefficient of the first stage is 1.05, 1.30, 1.30 and 1.1–1.50 at the aluminum distribution pattern of a uniform gradient, semi-gradient, single-gradient and double-gradient, the T.V of the first-stage molten slag is 1.90 wt.%, 0.49 wt.%, 0.45 wt.% and 0.32 wt.%, second-stage slag is 1.88 wt.%, 0.61wt.%, 0.79 wt.% and 0.63 wt.%, and the third-stage slag is 1.69 wt.%, 2.42 wt.%, 1.52 wt.% and 1.24 wt.%, respectively. The average T.V in the molten slag of the three stages is 1.82 wt.%, 1.17 wt.%, 0.92 wt.% and 0.73 wt.% at the comprehensive aluminum addition coefficient of 1.05, respectively. It is worth noting that the corresponding average T.V in the discharged residue slag (after cooling) of the three stages is 2.34 wt.%, 1.53 wt.%, 1.34 wt.% and 1.15 wt.%, respectively, which is higher than that of the on-line molten slag. As a result, excessive reducing agent is conducive to improving the thermodynamic conditions of aluminothermic reactions by increasing the aluminum addition coefficient of each smelting stage, which verifies the analysis in Section 3.1.1. The conduction time of SHS-EAH-2 by SiG-ADP reached $24.3 \text{ min}\cdot\text{t}^{-1}$, which is significantly longer than that of the other samples. The T.V of SHS-EAH-4 by DG-ADP is significantly lower than that of SHS-EAH-1 by U-ADP, while the conduction time was $16.5 \text{ min}\cdot\text{t}^{-1}$, which was slightly lower than that of SHS-EAH-1 by U-ADP. In conclusion, the multi-stage gradient aluminum distribution process can effectively decrease the T.V and conduction time, so as to achieve the purpose of improving the smelting yield and efficiency, and DG-ADP shows the best index characteristics.

Table 2. Different feeding methods and Al distribution coefficient (η).

Al Distribution Pattern	No.	η			Feeding Ratio	η	Average T.V in Molten Slag, wt.%				T.V in Discharged Slag, wt.%	Time, $\text{min}\cdot\text{t}^{-1}$
		1st Stage	2nd Stage	3rd Stage			1st Stage	2nd Stage	3rd Stage	Ave.		
Uniform	SHS-EAH-1	1.05	1.05	1.05	4:4:2	1.05	1.90	1.88	1.69	1.82	2.34	18.5
Semi-gradient	SHS-EAH-2	1.30	1.30	0.00	4:4:2	1.05	0.49	0.61	2.42	1.17	1.53	24.3
Single-gradient	SHS-EAH-3	1.30	1.00	0.65	4:4:2	1.05	0.45	0.79	1.52	0.92	1.34	17.3
Double-gradient	SHE-EAH-4	1.1–1.5	0.8–1.2	0.65	2 + 2:2 + 2:2	1.05	0.32	0.63	1.24	0.73	1.15	16.5

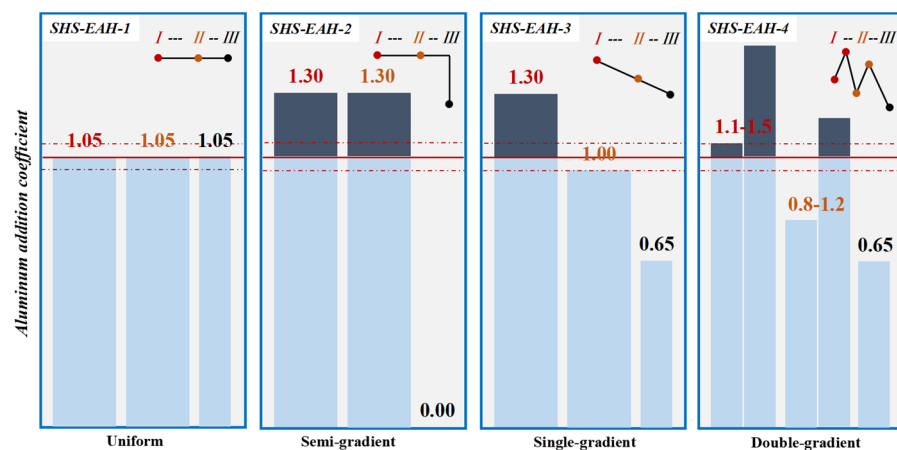


Figure 8. Aluminum distribution pattern of multi-stage SHS-EAH process.

The composition of FeV50 by different aluminum distributions was shown in Table 3. All the elemental compositions of FeV50 alloy from SHS-EAH-2 to SHS-EAH-4 meet the national standard of GB/T 4139-2012 (China) for FeV50-A by G-ADP, and the Al content of the prepared FeV50 alloy decreased significantly and the V content increased by the gradient aluminum distribution, which not only reduced the vanadium loss in the slag, but also improved the utilization ratio of Al.

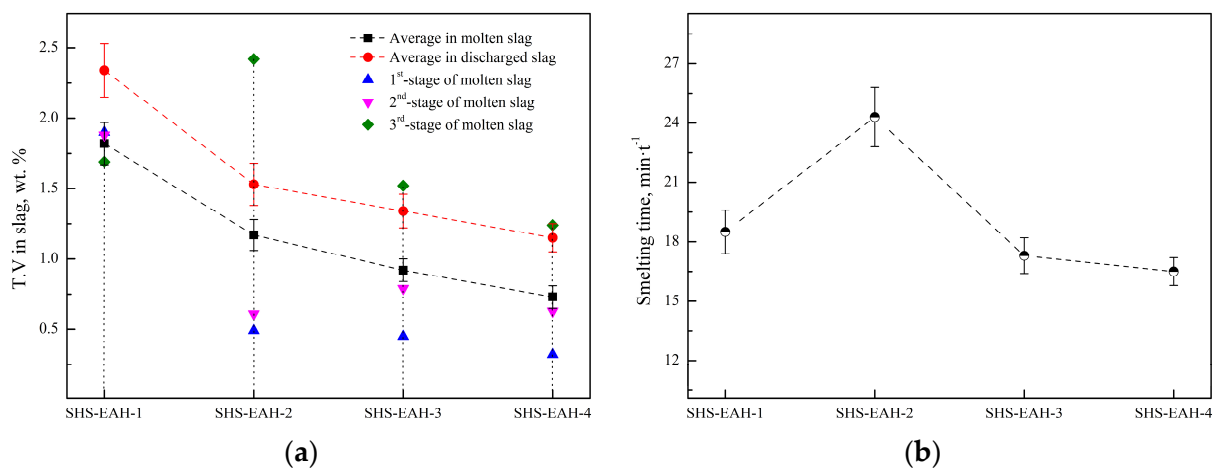


Figure 9. T.V in residue slag and conduction time by different aluminum distribution patterns. (a) T.V, (b) conduction time.

Table 3. FeV50 composition by different aluminum distribution coefficient.

No.	Elements and Content, wt.%						
	V	Fe	C	Si	P	S	Al
SHS-EAH-1	50.2	47.5	0.29	0.4	0.07	0.02	1.5
SHS-EAH-2	50.4	47.3	0.21	0.5	0.05	0.01	1.4
SHS-EAH-3	51.3	47.0	0.16	0.6	0.05	0.01	0.8
SHS-EAH-4	51.7	47.0	0.13	0.6	0.04	0.01	0.5
FeV50-A	48.0~55.0	--	≤0.4	≤2.0	≤0.06	≤0.04	≤1.5
FeV50-B	48.0~55.0	--	≤0.6	≤2.5	≤0.10	≤0.05	≤2.0

The above theoretical and experimental results indicate that the thermodynamic conditions of smelting have been effectively improved by redistributing the ingredient in each stage and combining multiple feeding and multiple smelting, while ensuring the constant comprehensive aluminum distribution coefficient for each furnace. Compared with the traditional uniform aluminum blending process, the MS-G-ADP process has shown significant advantages in the smelting yield, smelting efficiency and alloy composition control.

On the other hand, the T.V content of the discharged residue slag is significantly higher than that of the on-line molten slag in each stage, which was mentioned above. Taking SHS-EAH-4 for example, the T.V content of the three-stage residue slag by air cooling is 0.53 wt.%, 0.76 wt.% and 1.65 wt.%, while the T.V content in the corresponding molten slag is 0.32 wt.%, 0.63 wt.% and 1.24 wt.%, respectively. Through the SEM-EDS and MLA analysis of the residue slag in Figures 10 and 11, the mineral phases in the slag were composed of magnesium aluminum spinel, calcium aluminate, vanadium spinel and ferrovandium [36]. Vanadium is mainly combined with magnesium and aluminum to form a spinel structure in the existing state of isomorphism, and the reduced vanadium is precipitated at the grain boundary in the form of vanadium-rich spherical particles. The mass proportion of alloy in the three-stage slag is 0.06 wt.%, 0.13 wt.% and 1.01 wt.%, which indicates that the separation of the slag and alloy is not completed in the process of slag discharging and alloy casting, especially the casting in the third stage.

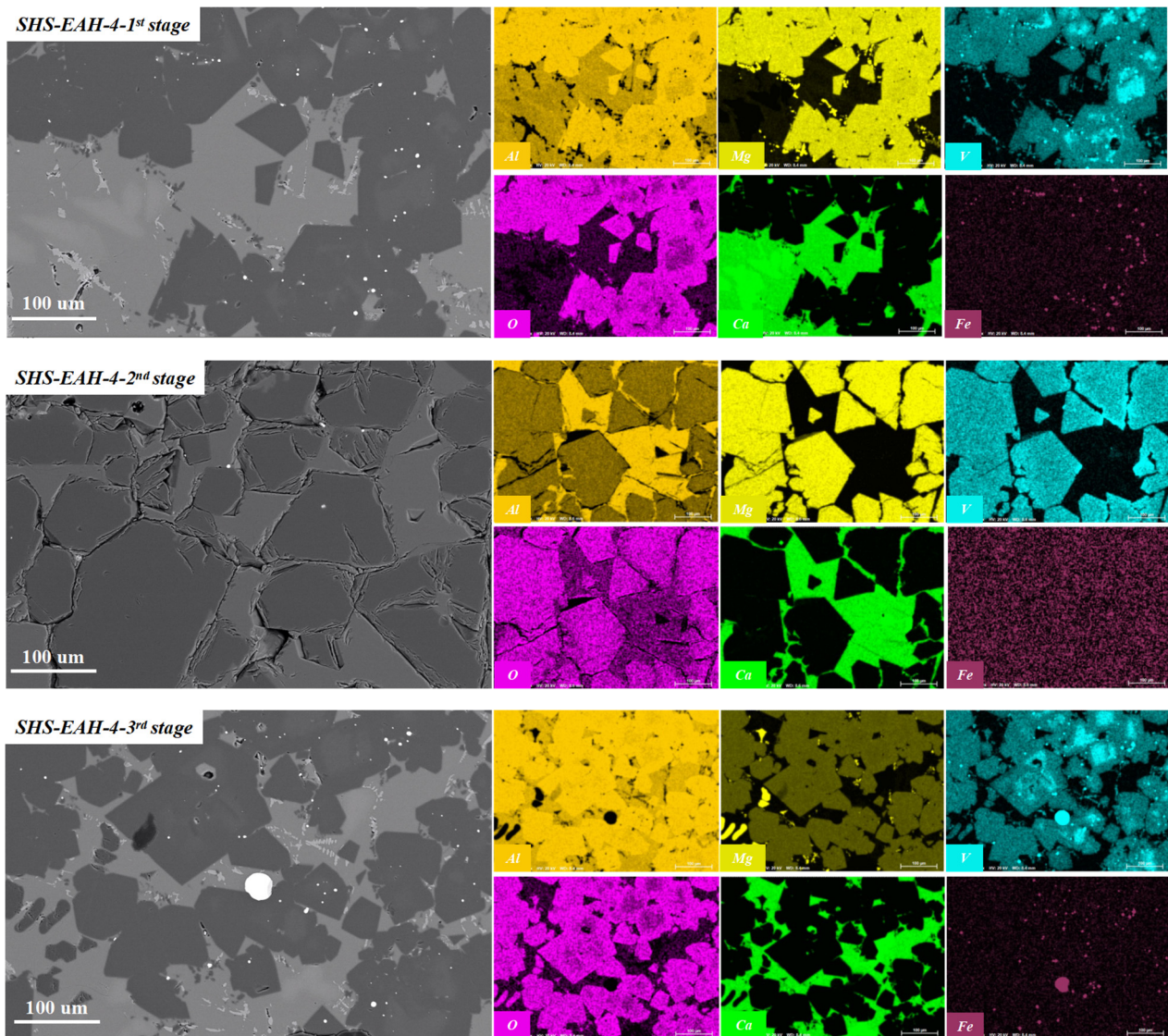


Figure 10. SEM analysis of residue slag of SHS-EAH-4 by DG-ADP.

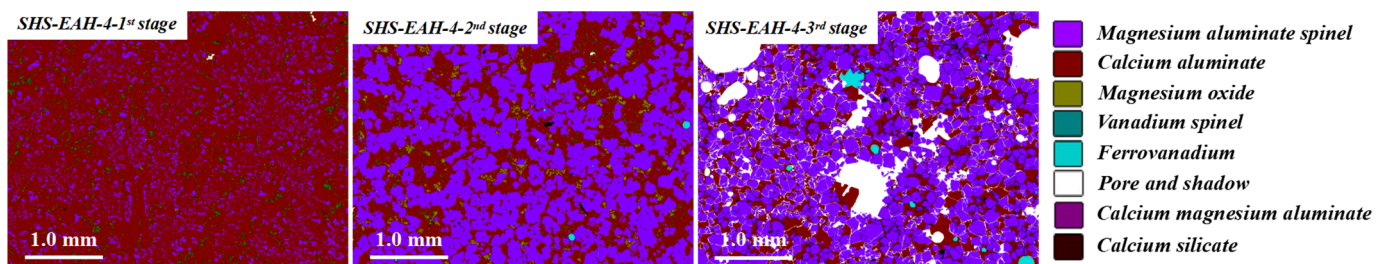


Figure 11. MLA analysis of residue slag of SHS-EAH-4 by DG-ADP.

3.2. Efficient Separation of Molten Slag and Alloy

3.2.1. Gravity Settlement during the Reducing Reaction

Spherical molten ferrovanadium particles are subjected to the combined action of gravity, buoyancy and resistance in a gravity field, when freely settled in an approximately infinite fluid [40]. The settlement equilibrium can be expressed by Equation (16). Taking the

settlement of the alloy particles with diameter d settling in the molten slag as an example, the gravity, buoyancy and resistance of the particles can be expressed in Equations (17)–(19).

$$G - F - f = ma \quad (16)$$

$$G = \pi \cdot d^3 \cdot \rho_m \cdot g / 6 \quad (17)$$

$$F = \pi \cdot d^3 \cdot \rho_s \cdot g / 6 \quad (18)$$

$$f = \pi \cdot \zeta \cdot d^2 \cdot \rho_s \cdot u_0^2 / 8 \quad (19)$$

where G , F and f with the unit N are the force of gravity, buoyancy and resistance on the settlement process, respectively; m is the mass of a spherical particle with a unit of kg; a is the acceleration of the spherical particle with a unit of $\text{m} \cdot \text{s}^{-2}$; ρ_m and ρ_s are the density of the alloy and slag, respectively, $\text{kg} \cdot \text{m}^{-3}$; g is the gravitational acceleration, $\text{m} \cdot \text{s}^{-2}$; ζ is the drag coefficient; u_0 is final settling velocity, $\text{m} \cdot \text{s}^{-1}$. The settlement process of the alloy particles is gradually accelerated until the resistance increases to be balanced with the change in the velocity. Due to the short acceleration time, it is considered that the settlement process always sinks at the final settlement velocity. When the acceleration value equals 0, Equation (20) can be obtained by substituting Equation (17) to Equations (16) and (19). The final settlement velocity expression can be expressed by Equation (21).

$$\pi \cdot d^3 \cdot (\rho_m - \rho_s) \cdot g = \pi \cdot \zeta \cdot d^2 \cdot \rho_s \cdot u_0^2 / 8 \quad (20)$$

$$u_0 = [4d \cdot (\rho_m - \rho_s) / 3\rho_s \cdot \zeta]^{1/2} \quad (21)$$

where ζ is the Reynolds number function of the relative motion of the fluid and particle. The resistance coefficient values corresponding to different Reynolds number (Re_0) intervals and the final settlement velocity are shown in Table 4. For the settlement of small-diameter spherical particles, the Re_0 value is generally less than 2.0, so the expression of the final settlement velocity in laminar flow, known as Stokes' law, is most widely used. According to the above analysis, the main factors affecting the separation of the molten slag and alloy include the slag thickness, slag characteristics, particle diameter and settlement time [41]. A low viscosity, high temperature, large particle size, thin slag thickness and long smelting time are conducive to the settlement of ferrovanadium.

$$\zeta = f(Re_0) \quad (22)$$

$$Re_0 = d \cdot u_0 \cdot \rho_s / \mu \quad (23)$$

Table 4. Resistance values for different Reynolds intervals.

Re_0	Fluid Type	ζ	Settlement Velocity	No.
≤ 2.0	Laminar region	$24/Re_0$	$u_0 = d^2 \cdot (\rho_m - \rho_s) \cdot g / 18\mu$	30
2.0~500	Transition region	$18.5/Re_0^{0.6}$	$u_0 = 0.27[d \cdot (\rho_m - \rho_s) \cdot g Re_0^{0.6} / \rho_s]^{1/2}$	31
500~ 2×10^5	Turbulent region	0.44	$u_0 = 1.74[d \cdot (\rho_m - \rho_s) \cdot g / \rho_s]^{1/2}$	32
$\geq 2 \times 10^5$	—	0.1	--	--

At the end of smelting, after discharging and casting, the mixed molten slag and alloy will be separated during the melt solidification. Stokes' law can be used to analyze and calculate the physical separation process. The chemical composition of typical slag samples of an Al_2O_3 - MgO - CaO -based system was analyzed by X-ray fluorescence spectroscopy (XRF), and the velocity of the molten slag at 1900 °C and the melting point were predicted by the "Velocity module" and "phase diagram" in FactSage 8.0. As can be seen from Table 5, the viscosity of typical industrial slag samples by the SHS-EAH process ranges from 0.40 Pa·s to 0.54 Pa·s at 1900 °C. The viscosity of the molten slag increases with the increase in Al_2O_3 and CaO , while it decreases with the increase in MgO . In addition, the

melting point of typical industrial slag samples ranges from 1650 °C to 1810 °C; reducing lining erosion and increasing lime dosage is conducive to reducing the melting point of slag.

Table 5. Theoretical viscosity of typical slag sample.

No.	Slag Composition, wt.%					Viscosity, Pa·s	Melting Point, °C
	SiO ₂	Al ₂ O ₃	CaO	MgO	Fe ₂ O ₃		
S-1	0.6	61.5	21.3	15.5	1.1	0.43	1650
S-2	0.8	61.0	15.3	21.2	1.7	0.40	1740
S-3	0.5	65.2	19.8	13.0	1.5	0.46	1670
S-4	0.6	65.4	13.1	19.5	1.4	0.44	1780
S-5	0.5	71.3	18.7	8.1	1.4	0.54	1660
S-6	0.6	71.6	10.8	15.4	1.6	0.50	1810

Assuming that the gravity settlement of alloy particles is in the laminar flow zone (Re_0 less than 2.0) at a slag thickness of 0.30 m and a smelting temperature of 1900 °C, Equation (30) is therefore adopted to predict the settlement velocity and settlement time with a different particle size in the viscosity range from 0.40 to 0.54 Pa·s, which is shown in Table 6. According to Table 6, the theoretical settlement time of the alloy and corresponding floating time of the slag with a diameter of 0.50 mm is 5.7 min and 0.03 min under industrial conditions, respectively. In order to ensure the efficient settlement of fine alloy particles under the same conditions, continuous electrification should be carried out after the completion of the reducing reaction to maintain the system in a molten state. If the settlement of the alloy is controlled effectively, the slag inclusion of the alloy can be effectively avoided.

Table 6. Theoretical settlement characteristics of ferrovanadium at 1900 °C.

Type	Viscosity, Pa·s	ρ , g·cm ⁻³	d , mm	u_0 , m·s ⁻¹	Re_0	t , min
alloy	0.54	7.0	0.10	3.53×10^{-5}	2.29×10^{-5}	141.7
	0.54	7.0	0.50	3.53×10^{-3}	2.29×10^{-2}	5.7
	0.40	7.0	0.10	4.76×10^{-5}	4.17×10^{-5}	104.9
	0.40	7.0	0.50	4.76×10^{-3}	4.17×10^{-2}	4.2
slag	0.0025	3.5	0.10	7.62×10^{-3}	1.07	0.66
	0.0025	3.5	0.50	0.76	1067	0.03

3.2.2. Efficient Separation of Slag and Alloy

The distribution of the T.V and T.Fe (total ferrum) in the residue slag at different smelting stages is shown in Figure 12. As can be seen from Figure 12a, the T.V and T.Fe in the refining slag (first stage and second stage) is relatively low, while the corresponding mass content in the casting slag (third stage) shows a trend of significant increase. Through the phase cleavage analysis of the casting slag, an obvious spherical rich area of vanadium and iron was found (Figure 12b). The total mass fraction of the vanadium and iron is more than 95.0 wt.%, which is considered as the primary reduction alloy, and is consistent with the conclusions made in Section 3.2.1.

After optimizing the aluminum addition coefficient of each stage, the main influencing factors affecting the separation of the slag and alloy were investigated based on the industrial production performance. As can be seen from Figure 13, the T.V content of the residue slag decreases with the decrease in the viscosity and increases with the increase in the melting point of the slag. In the process of industrial production, the main components of molten slag are composed of 65.0 wt.% Al₂O₃, 15.0 wt.% CaO and 20.0 wt.% MgO, which is similar to that of sample S-4 in Section 3.2.1. The viscosity and melting point of the slag are about 0.46 Pa·s and 1780 °C, respectively, while the corresponding T.V content is 1.33 wt.%. It is beneficial to reduce the T.V content by increasing the CaO addition and optimizing the knot strength of the furnace to improve the slag characteristics. According

to Figure 14, decreasing the slag thickness and increasing the casting temperature and the insulation thickness are conducive to the settlement of alloy particles and the decreasing of vanadium loss. When the slag thickness decreased from 54.9 cm to 30.2 cm, the T.V in the residue decreased from 1.56 wt.% to 0.85 wt.%. When the casting temperature increased from 1829 °C to 1972 °C, the T.V in the residue decreased from 1.96 wt.% to 0.88 wt.%. While when the isolation thickness increased from 0 cm to 15.0 cm, the corresponding T.V in the residue decreased from 1.41 wt.% to 0.62 wt.%. In conclusion, the separation efficiency of the slag and alloy was obviously improved, and the average T.V in the residue slag decreased from 1.15 wt.% to 0.65 wt.% at the slag approximate composition of Al_2O_3 65.0 wt.%, CaO 18.0 wt.%, MgO of 15.0 wt.%, and slag discharging rate of 80.0 wt.%, casting temperature of 1950 °C and insulation thickness of 15 cm.

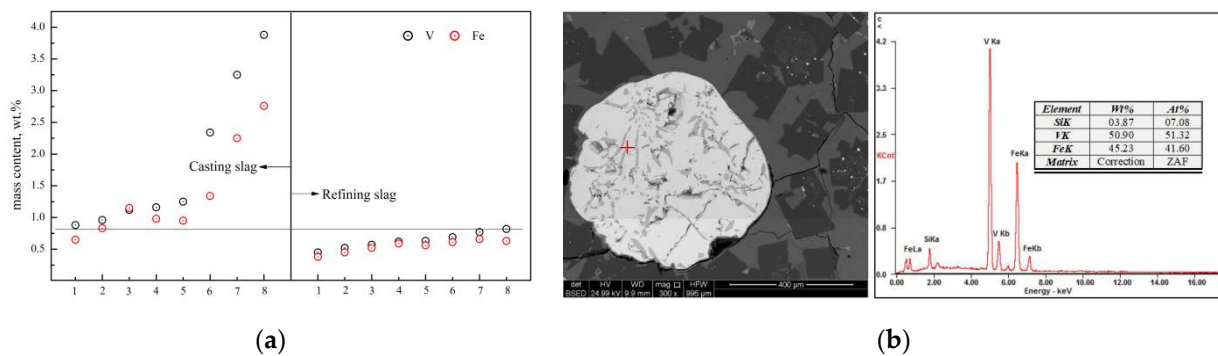


Figure 12. Typical distribution of V and Fe in slag. (a) Distribution of T.V and T.Fe in slag. (b) Alloy and composition of casting slag.

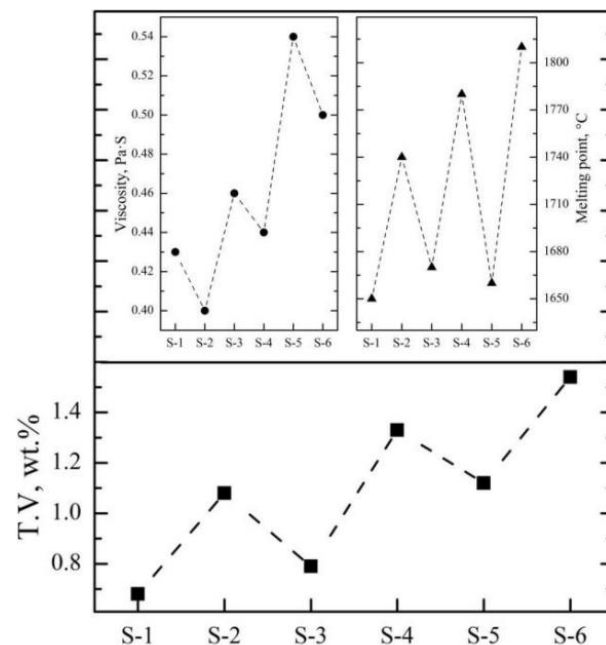


Figure 13. Effect of slag characteristics on T.V in slag.

According to the MLA and XRD results in Figures 15 and 16 and Table 7, the main equilibrium phases are $\text{MgO}\cdot\text{Al}_2\text{O}_3$, $\text{CaO}\cdot\text{Al}_2\text{O}_3$, $\text{CaO}\cdot 2\text{Al}_2\text{O}_3$ and $\text{CaO}\cdot\text{TiO}_2$. The proportion of $\text{MgO}\cdot\text{Al}_2\text{O}_3$ increases with the prolongation of the smelting time due to the increased lining erosion. Vanadium mainly coexisted with $\text{MgO}\cdot\text{Al}_2\text{O}_3$ as a solid solution and ferrovanadium. The formation of $\text{CaO}\cdot\text{TiO}_2$ in slag is mainly due to the process of the acid extraction of vanadium from vanadium oxide materials and the introduction of titanium impurities. On the whole, the alloy particles presented in slag, especially the

last smelting stage, caused by the incomplete separation of the slag and alloy decreases significantly compared with that before optimization.

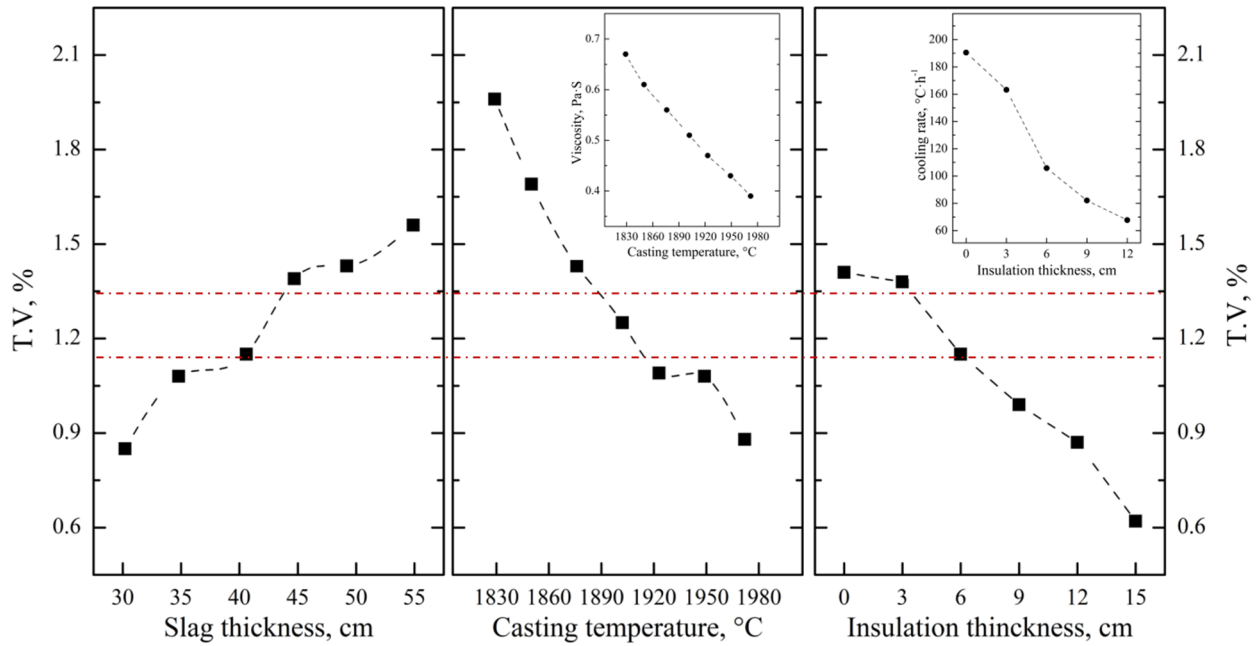


Figure 14. Effect of slag thickness, casting temperature and insulation thickness on T.V in slag.

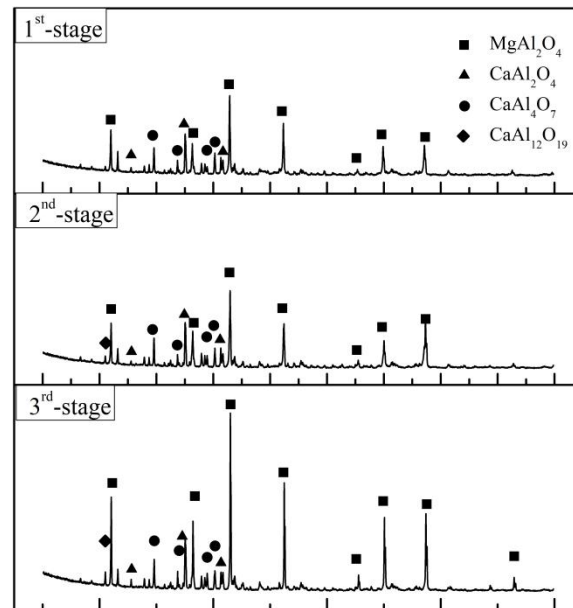


Figure 15. XRD diffraction of residue slag.

Table 7. Mineral composition and content of residue slag in different smelting stage after process optimization.

No.	Mineral Composition and Content, wt.%					
	MgO·Al ₂ O ₃	CaO·Al ₂ O ₃	CaO·2Al ₂ O ₃	CaO·6Al ₂ O ₃	Ferrovandium	Perovskite
SHS-EAH-4-I	53.32	9.24	35.22	0.00	0.00	2.12
SHS-EAH-4-II	45.73	18.79	33.05	0.00	0.00	2.43
SHS-EAH-4-III	56.25	10.40	25.82	0.00	0.73	2.89

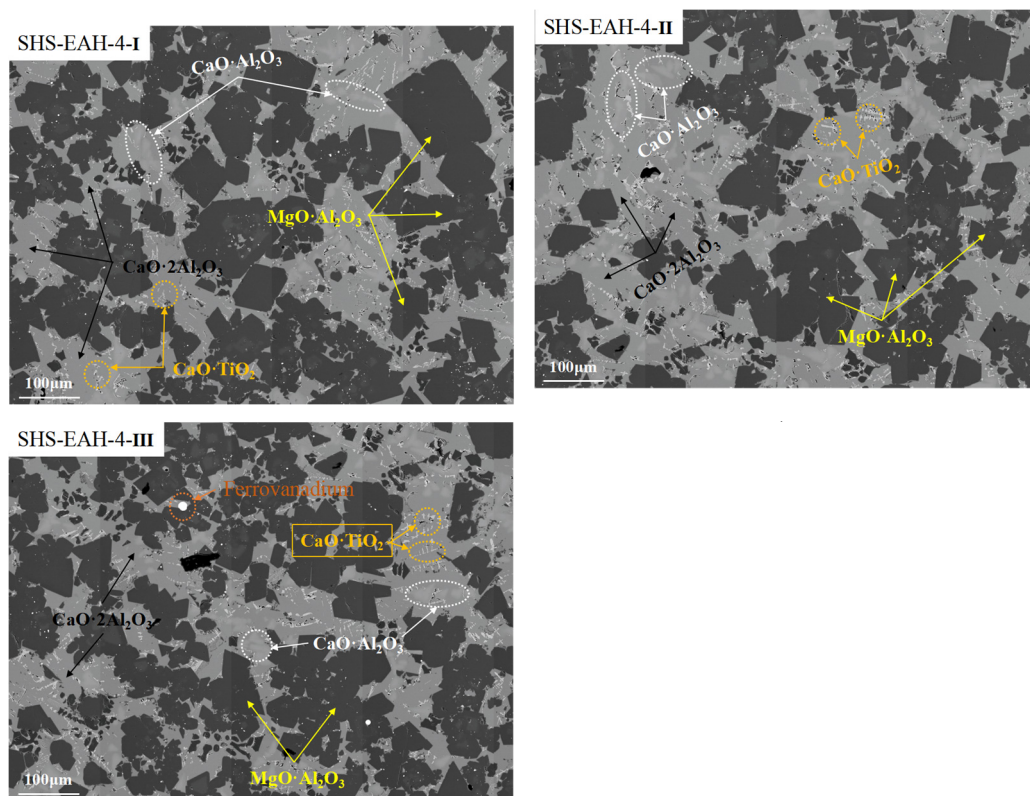


Figure 16. Micrograph of residue slag in different smelting stage by MLA system.

The analysis results of the infinite fluid free settling theory indicate that the main influencing factors of the separation of the molten slag and alloy include the slag characteristics, slag thickness, particle diameter and settlement time. The thermodynamic and kinetic conditions of the ferrovanadium smelting process have been effectively improved by optimizing and adjusting the process parameters of the material structure, slag composition, system superheat and discharge controlling. Compared with traditional processes, the use of a new secondary casting mixing and efficient settling process demonstrates significant advantages in the deep reduction of vanadium oxides and the efficient separation of the reduction products.

3.3. Impurity Control and Secondary Resources in On-Line Circulation

3.3.1. Impurity Control Principle

The typical inclusions of the national standards can be divided into metal inclusions and non-metal inclusions. The metal inclusions mainly include Mn and Al, while the non-metal inclusions mainly contain C, Si, P and S. These inclusions need to be defined and controlled during the preparation of ferrovanadium.

Al, as the reducing agent in the reducing smelting process of FeV50 and FeV80, mainly depends on the accuracy of the ingredients. Too much aluminum addition will lead to excessive Al in the alloy. On the contrary, it is not beneficial to the reduction of vanadium oxides when there is not enough aluminum. Therefore, an accurate batching model was established in Section 2.3 to control the reduction effect and predict the aluminum content in the alloy. If the Al content exceeds the standard requirements of the alloy, a de-aluminizing operation should be carried out by adding strengthening oxidizer without introducing new impurities, such as vanadium oxides and iron oxides. Fe and Mn are weakly reducing metals; iron oxides and manganese oxides in the raw materials can be therefore be reduced to the metallic state and settled into the alloy, according to Figure 17.



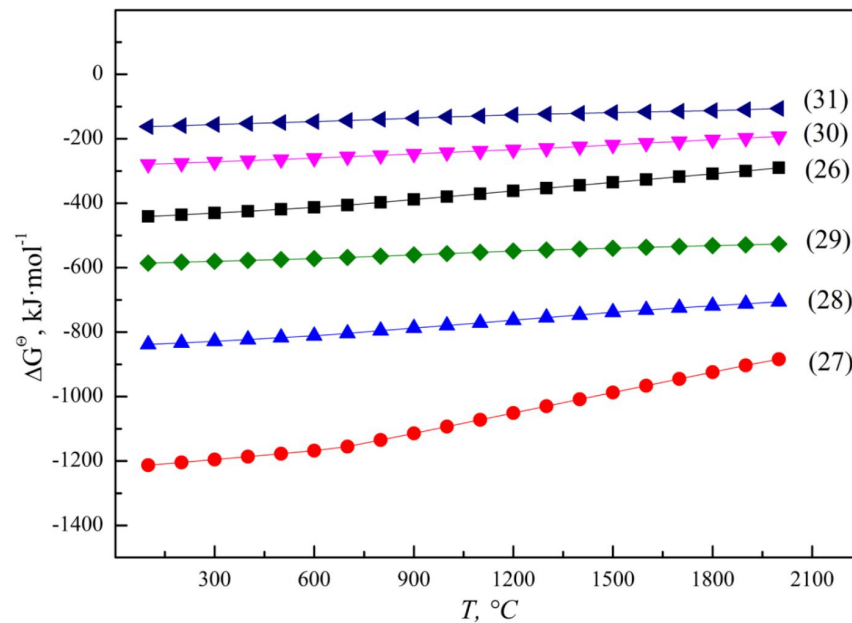
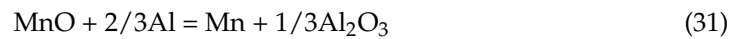
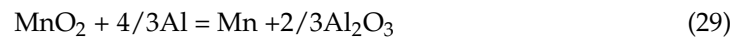
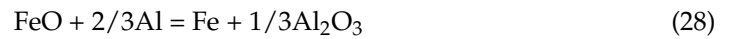
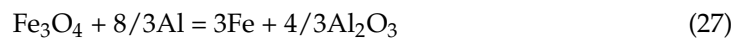
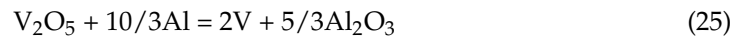
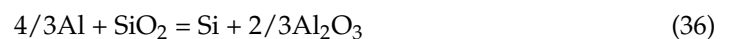
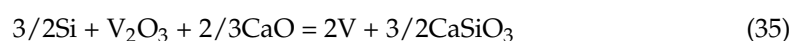
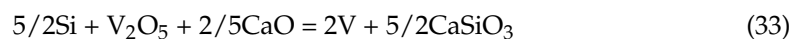


Figure 17. ΔG^\ominus for thermite reactions of Fe and Mn oxides.

Similar to Fe and Mn, Si is a weak reducing non-metallic substance, which can be used as a reducing agent to reduce vanadium oxides under certain conditions. When heated to above 1700 °C, V_2O_3 or V_2O_5 undergoes silicothermic reduction to produce ferrovanadium via the reactions of 32~36 and Figure 18. It is important to note that Si does not have the thermodynamic feasibility to reduce low-valence vanadium oxides without the addition of CaO, and the reduced by-products have the disadvantages of easy pulverization, which easily causes environment risks. Thus, the silicothermic reduction process is an unsustainable industrialized technology, which has been almost completely eliminated. On the other hand, SiO_2 in raw materials or after oxidation will be theoretically reduced in alloys in the aluminothermic reduction system.



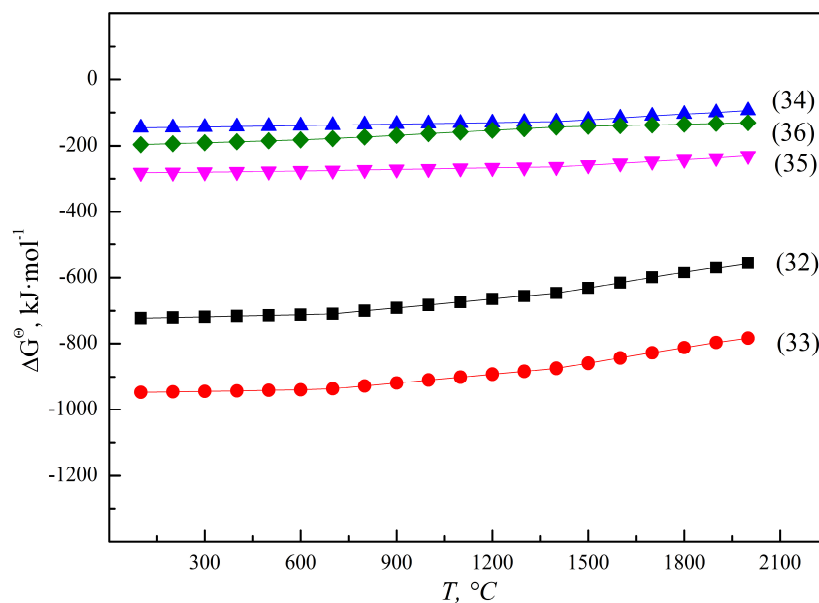
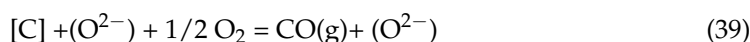
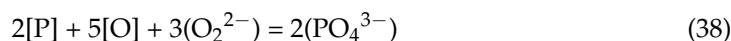


Figure 18. ΔG^\ominus for thermic reactions of vanadium and silicon oxides.

According to the phase diagram of C, P and S of the V-Fe-O system at 1800 °C in Figure 19, P does not have metallic properties and is generally difficult to find as an independent elementary substance in metal or alloy melts. The kinetic hot zones of dephosphorizing reactions are mainly concentrated in the interface of the slag and alloy, and generate phosphate into the slag phase by combining with strong alkaline oxides. High alkalinity, strong oxidation, low viscosity and appropriate temperature are beneficial to dephosphorization [42]. Similar to the principle of dephosphorization, during desulfurization, S is also removed by the slag at an oxygen potential above 1.0×10^{-4} atm. When the desulfurization product enters slag, it is further decomposed and gasification. High alkalinity, weak oxidation, low viscosity and high temperature are conducive to desulfurization. C easily reacts with free oxygen in the melt to form carbon oxides; improving the activity of free oxygen is conducive to decarbonization. Actually, in industrial production, the decarbonization reaction usually competes with other redox reactions between carbon and metals, including alkali metals, alkali earth metals and transition metals. According to the reducibility, C has the ability to reduce some transition metals, such as vanadium oxides and iron oxides. The removal mechanism of the above non-metallic inclusions is as follows. In addition, the unremoved C, P and S in the alloy mainly occur as V_2C , FeP_2 , FeO_4P or FeS through the “Predom Module” of FactSage 8.0.



3.3.2. Industrialization Control Standard of Raw Material Impurities

Through the statistical analysis of the impurities of the alloy and the corresponding raw materials in Figure 20, the content of the impurities in the alloy is basically in a positive correlation with that in the raw materials. More than 80.0 wt.% of the Si and Mn in the alloy were reduced in the case of an excessive aluminum coefficient. S is always at a low level in the alloy and does not increase significantly with the corresponding impurity content of the raw materials, which has a certain randomness. Based on the analysis of the reduction reaction and slag characteristics, the favorable thermodynamics conditions for desulfurization (high temperature, high alkalinity and low oxidation) and dephosphorization (low temperature, high alkalinity and high oxidation) were determined.

Therefore, favorable thermodynamic conditions for the removal of S, but not P, were actually achieved. In industrial processes, the thermodynamic conditions of dephosphorization can be satisfied as far as possible under the premise that S is fully controllable.

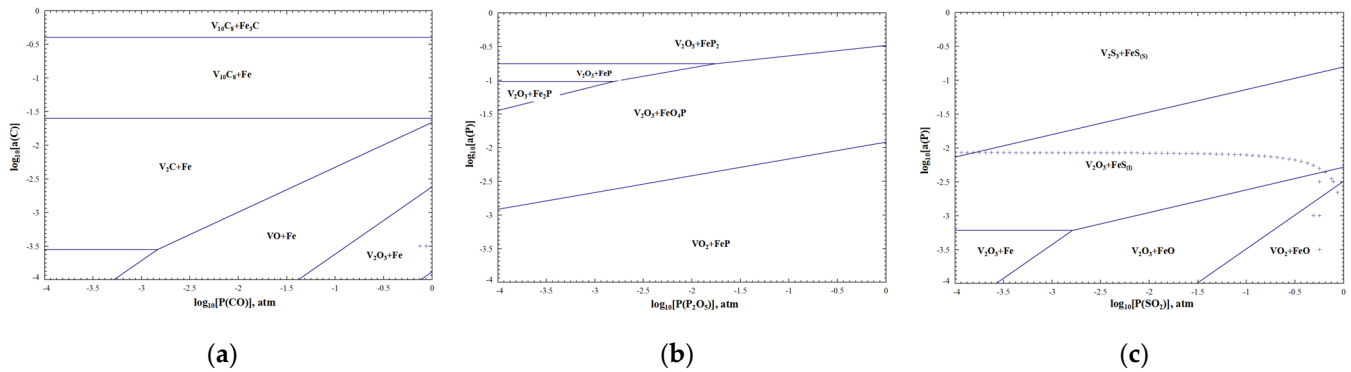


Figure 19. Phase diagram of C, P, S of V-Fe-O system at 1800 °C. (a) V-Fe-C-O; (b) V-Fe-P-O; (c) V-Fe-S-O.

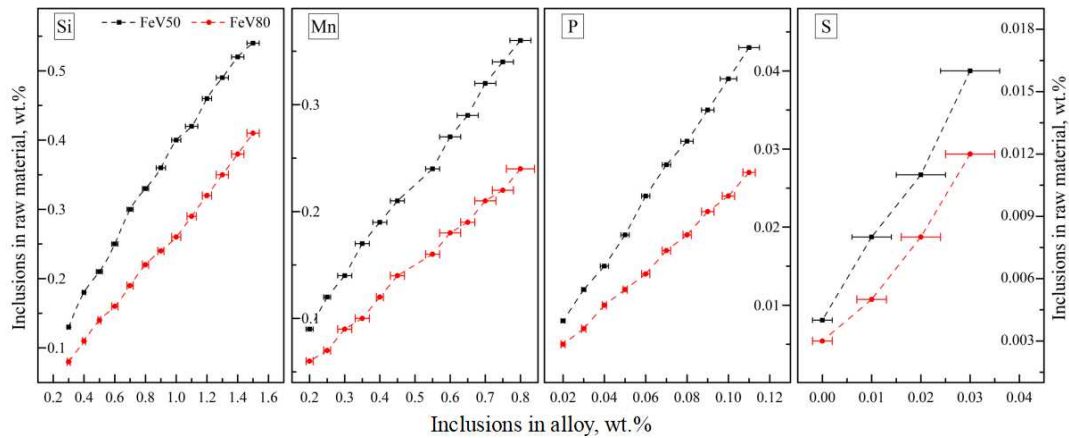


Figure 20. Relation of inclusions between raw materials and ferrovanadium.

According to the distribution relation of inclusions between raw materials and alloy, the impurities controlling the standard of mixed raw materials for different ferrovanadium grades was established. As can be seen from Table 8, the upper limitation of FeV50-A and FeV80-A for Si, Mn, P and S are 0.50 wt.%, 0.20 wt.%, 0.017 wt.% and 0.04 wt.% and 0.30 wt.%, 0.12 wt.%, 0.01 wt.% and 0.04 wt.%, respectively. The distribution mass ratio of Si, Mn, P, and S entering the alloy is 85.1~92.6 wt.%, 92.3~95.7 wt.%, 72.5~82.3 wt.% and 0~42.7 wt.%, respectively.

Table 8. Inclusions controlling standard of different ferrovanadium grades.

Grades	Inclusion Composition Control Limitation of Raw Material, wt.%				
	Si	Mn	P	S	C
FeV50-A	0.50	0.20	0.017	0.04	0.6
FeV50-B	0.50	0.20	0.032	0.06	0.8
FeV80-A	0.30	0.12	0.010	0.04	0.3
FeV80-B	0.30	0.12	0.015	0.06	0.5
Distribution ratio, wt.%	85.1~92.6	92.3~95.7	72.5~82.3	0~42.7	—

Through the analysis of typical impurity removal mechanisms and distribution characteristics during the smelting of ferrovanadium mentioned above, the control standards for

the impurity components of raw materials in different grades of alloy have been obtained, and detailed data have been provided for the online circulation of vanadium-bearing secondary resources. Compared with traditional process, this study has significant advantages in the adaptability of complex raw materials, product quality stability and comprehensive utilization of secondary resources.

4. Evaluation of the Promoted SHS-EAH Process

4.1. Evaluation of Technical and Economic Indicators

Based on the distribution rules and control standards established above, a new smelting process is proposed for the site of the vanadium extraction plant in Figure 21. In the process, 86.2 wt.% of the vanadium sources are supplied by vanadium oxides from the vanadium slag plant, while the rest of the vanadium sources are recycled by 0.6 wt.% of collected dust, 0.7 wt.% of vanadium-rich residue slag, 1.2 wt.% of precipitator dust and 11.3 wt.% of sub-quality alloy from the smelting plant. A total of 56.0 wt.% of the iron resources are supplied by BMIG from the vanadium slag plant. From the economic perspective, the process is feasible as long as heat waste can be reasonably utilized. During the industrial smelting process, the slag of the three smelting stages makes up 15.9%, 15.9% and 20.6% of the reaction and electric auxiliary heat in the furnace, respectively. And the heat is taken away for the heating the leaching liquid of the vanadium extraction plant from 25 °C to 60 °C. On the other hand, the cooled corundum slag is used in the preparation of industrial refractory materials and raw materials for replenishing the tilting furnace. With this proposed industrial waste treatment process, vanadium-bearing and ferrous-bearing secondary resources are effectively recycled and utilized, and the impurity elements of the alloy are effectively controlled.

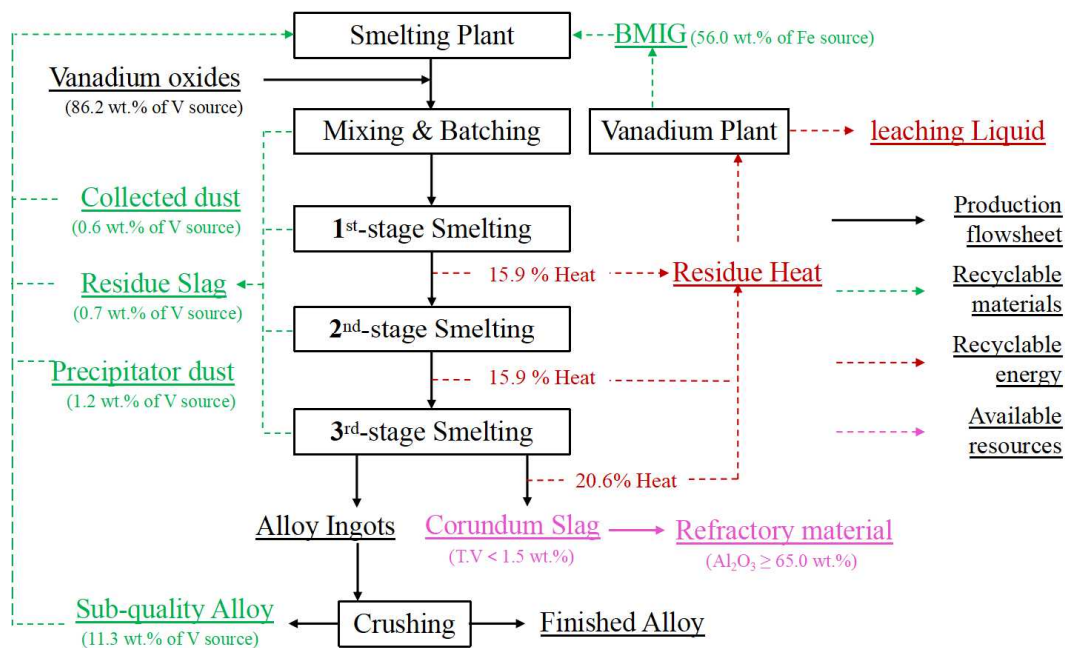


Figure 21. Flowsheet of on-line cycle for the ferrovanadium smelting process.

Through the in-depth analysis of the preparation theory of the ferrovanadium alloy and the optimization control of the technological conditions, the reduction of vanadium, separation of slag and alloy, and comprehensive utilization of secondary resources have been significantly improved. At present, the new multi-stage double-gradient battering and smelting process of DG-ADP has been fully applied and promoted in PG Group(XC) in China. The internal circulation of the vanadium-bearing materials in the ferrovanadium smelting system and the external circulation of the iron and residue slag applied in the same system are established, and the zero discharge of solid and liquid waste from ferrovana-

dium production line has been achieved. Compared with other typical ferrovanadium preparation enterprises listed in Table 9 and Figure 22, the new process has significant advantages in terms of the smelting yield, smelting efficiency, aluminum consumption, product quality and other aspects. On the one hand, the key technology of the intensive smelting and separation of ferrovanadium is proposed based on the V-Al-O reduction equilibrium theory and the infinite fluid-free sedimentation theory, which enabled the deep reduction of the vanadium in the slag and the efficient separation of the slag–alloy. The T.V content in the slag was reduced from 2.34 wt.% to 0.60–0.90 wt.%, and the slag–alloy ratio was reduced from 1.35 to 1.10. The corresponding smelting yield increased from 93.7 wt.% to 98.0–98.7 wt.% and the aluminum consumption decreased from 510 kg·t^{−1} to 400–420 kg·t^{−1}. On the other hand, based on the establishment of the precise batching model, the on-line circulation of the vanadium-bearing secondary resources and low-cost raw material replacement are realized, and the product quality was further effectively predicted and controlled. The utilization rate of the secondary resources and the substitution rate of low-cost raw materials reach 100%.

Table 9. Comparison of key technical indexes of typical ferrovanadium manufacturers.

Technical Indicator	Manufacturing Enterprise					
	PG Group (BH) China	PG Group (PZH) China	CG Group (CG) China	Hayveld (HV) South Africa	Evraz (E) Russia	PG Group (XC) China
Industrialization process	One-step			Multi-stage		
Al distribution pattern	Uniform			Uniform	Gradient	
Smelting unit	Straight tube furnace			Tilting furnace		
Vanadium source	V ₂ O ₅	V ₂ O ₃ + V ₂ O ₅	V ₂ O ₃ + V ₂ O ₅			
T.V in residue slag, wt.%	0.6~0.8	1.2~1.6	1.4~1.6	1.4~1.6	1.2~1.4	0.6~0.9
Slag–alloy ratio (FeV50)	1.25	1.00	1.25	1.25	1.25	1.10
Vanadium loss, wt.%	1.5~2.0	2.4~3.2	3.5~4.0	3.5~4.0	3.0~3.5	1.3~2.0
Smelting yield, wt.%	98.0~98.5	96.8~97.6	96.0~96.5	96.0~96.5	96.5~97.0	98.0~98.7
Elc consumption, kWh·t ^{−1}	250~300	800~900	300~350	300~350	500~600	900~1000
Aluminum coefficient	1.05~1.10	1.05~1.10	1.05~1.10	1.05~1.10	1.05~1.10	1.05~1.08
Al consumption, kg·t ^{−1}	520~540	410~430	510~530	510~530	510~530	400~420
Product controllability	Uncontrollable			Divinable and controllable		

4.2. Outlook and Challenges

In addition to the abovementioned process technical indicators significantly improved in Section 4, the novel SHS-EAH process with multi-stage G-ADP shows other advantages via the automation of process flow, stability of process, etc., which is conducive to the achievement of equipment automation, production intelligence and product customization. The produced alloy successfully meets the requirements of customized alloys such as low aluminum and low Mn according to different customers' needs. Based on the characteristics of the novel technology and equipment, a set of refining furnaces can be equipped to achieve a duplex smelting process of a tilting furnace combined with a refining furnace, which can reduce the smelting time and T.V in the slag, and further improve the smelting yield and efficiency. Taking the long view, this technology is not only suitable for the production of ferrovanadium alloy, but also can be extended to other enterprises that use aluminothermic reduction to prepare precious metals or alloys.

Furnace lining erosion is the core common technical problem in the preparation of superalloys. Taking the preparation of vanadium alloy as an example, the melting temperature of the smelting system is generally higher than 2000 °C and the instantaneous temperature can even reach 2500 °C, which will lead to the very strong scouring and erosion of the solid furnace lining. Such a situation will not only seriously worsen the slag characteristics, but also affect the furnace lifetime and reduce the production efficiency. This is the major limitation of the transition from the semi-continuous to continuous production of a tilting furnace for the preparation of vanadium alloy. How to achieve the melting point

of the slag to enable the melting of the alloy through the selection of lining materials and technical optimization is the main problem and challenge at present.

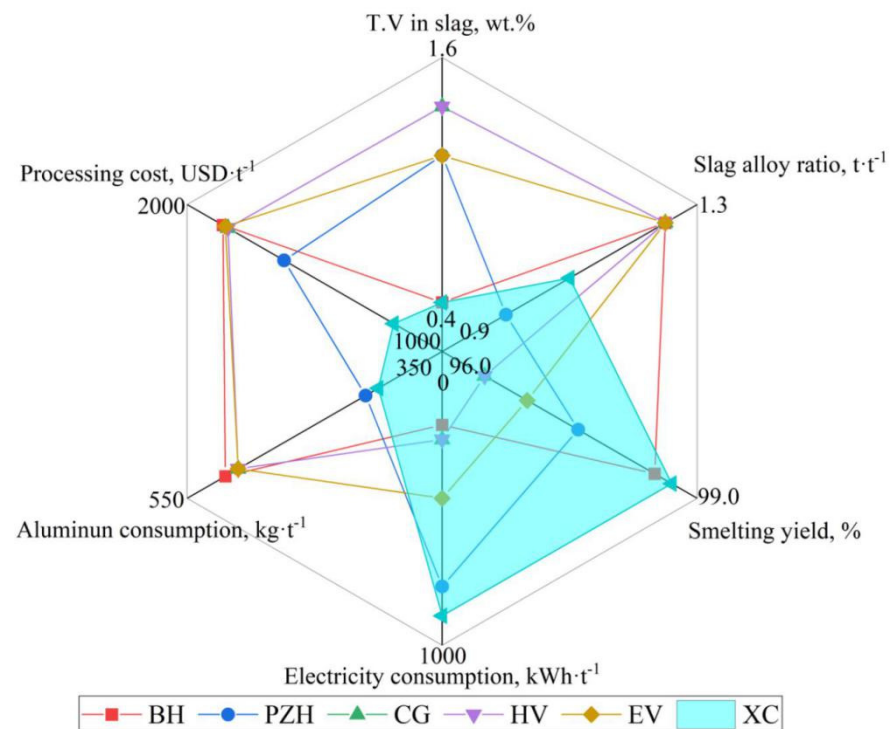


Figure 22. Brief evaluation of economic and technical indicators generated from the promoted SHS-EAH process.

5. Conclusions

In this work, a high-efficiency industrialized clean production technology for ferrovanadium based on multi-stage gradient batching and smelting was creatively proposed. The thermodynamic mechanism of aluminothermic reduction equilibrium, alloy settlement and inclusion controlling were derived. DG-ADP with the internal circulation of vanadium-bearing materials in a ferrovanadium smelting system and the external circulation of iron and residue slag applied in the same system is established in this optimized process, and the zero discharge of solid and liquid waste from the ferrovanadium production line has been achieved. A double-gradient aluminum addition pattern (DG-ADP), the high-efficiency separation of molten slag and alloy and control standard of typical impurity composition of raw materials were achieved with the improved SHS-EAH process. Through the optimization control of the technological conditions and evaluation of the key technical indicators of the new process, the reduction efficiency, separation efficiency and the comprehensive utilization rate of secondary resources has been significantly improved. In a word, this work reduced the whole T.V content in the industrially produced residue slag from 2.34 wt.% to 0.60 wt. %, the corresponding smelting yield increased from 93.7 wt.% to 98.7 wt.% and the aluminum consumption decreased from 510 kg·t⁻¹ to 400 kg·t⁻¹. In addition, the on-line circulation of the vanadium-bearing secondary resources and low-cost raw material replacement were realized and the product quality was further effectively controlled and improved. Therefore, this optimized process can enable high-efficiency industrialized vanadium smelting from different vanadium-bearing resources and provides a new insight for the cleaner production of ferrovanadium.

Author Contributions: Conceptualization, B.Y., J.S.; methodology, N.W., H.C., R.L., M.Y., L.G., D.Y. and L.Z. (Lei Zhang); software, H.C., N.W., R.L., M.Y., D.X., X.Y. and L.Z. (Lei Zhang); validation, R.L., M.Y., H.C., D.X. and D.Y.; formal analysis, T.Y., J.S., L.Z. (Lin Zhang) and D.Y.; investigation, C.J., D.X., H.C., M.Y., L.Z. (Lin Zhang), D.Y. and L.Z. (Lei Zhang); resources, L.G. and X.Y.; data curation,

J.S., N.W. and L.G.; writing—original draft preparation, B.Y., N.W. and X.Y.; writing—review and editing, B.Y., C.J., H.C., R.L., M.Y., D.X., L.G., X.Y., D.Y. and L.Z. (Lei Zhang); supervision, T.Y. and J.S.; project administration, J.S.; funding acquisition, J.S. All authors have read and agreed to the published version of the manuscript.

Funding: This work was financially supported by the National Natural Science Foundation of China (No. 52204310), China Postdoctoral Science Foundation (No. 2020TQ0059, No. 2020M570967). The authors wish to thank Pan Steel Group for providing help during this research.

Data Availability Statement: The data presented in this study are available in article.

Conflicts of Interest: Authors Lin Zhang and Xiong Yang were employed by the company Pangang Group Vanadium & Titanium Resources Co., Ltd. The remaining authors declare that the research was conducted in the absence of any commercial or financial relationships that could be construed as a potential conflict of interest.

References

1. Aarabi, K.M.; Rashchi, F.; Mostoufi, N.; Vahidi, E. Leaching of vanadium from LD converter slag using sulfuric acid. *Hydrometallurgy* **2010**, *102*, 14–21. [[CrossRef](#)]
2. Ulmer, U.; Asnao, K.; Patyk, A. Cost reduction possibilities of vanadium-based solid solution-microstructural, thermodynamic, cyclic and environmental effects of ferrovanadium substitution. *J. Alloys Compd.* **2015**, *648*, 1024–1130. [[CrossRef](#)]
3. Zhang, X.P.; Kou, G.J.; Wu, C.J. Effect of ferrovanadium inoculation on microstructure and properties of high speed steel. *China Foundry* **2008**, *5*, 95.
4. Dou, T.; Wu, Z.; Mao, J.F. Application of commercial ferrovanadium to reduce cost of Ti-V-based BCC phase hydrogen storage alloys. *Mater. Sci. Eng. A* **2008**, *476*, 34. [[CrossRef](#)]
5. Choi, C.; Kim, S.; Kim, R.; Choi, Y.; Kim, S.; Jung, H.; Yang, J.H.; Kim, H.T. A review of vanadium electrolytes for vanadium redox flow batteries. *Renew. Sustain. Energy Rev.* **2017**, *69*, 263–274. [[CrossRef](#)]
6. Sestager, K.A.; Alibek, Z.M.; Juan, M.G.; Olga, S.B.; Olga, Y.G.; Natalia, Y.G.; Elena, A.P. Kinetics of the synthesis of aluminum boride by the self-propagating high-temperature synthesis method. *Ceramics* **2022**, *5*, 435–446.
7. Lee, J.C.; Kim, E.Y.; Chung, K.W.; Kim, R.; Jeon, H.S. A review on the metallurgical recycling of vanadium from slags: Towards a sustainable vanadium production. *JMR&T* **2021**, *12*, 343–364.
8. Li, H.W.; Li, X.; Bu, X.P.; Chen, S.J. Prediction of the vanadium content of molten iron in a blast furnace and the optimization of vanadium extraction. *Separations* **2023**, *10*, 521. [[CrossRef](#)]
9. Huang, W.J.; Liu, Y.J. Crystallization behavior and growth mechanisms of spinel crystals in vanadium-containing slags. *ISIJ Int.* **2020**, *60*, 2183–2190. [[CrossRef](#)]
10. Wang, S.; Guo, Y.F.; Zheng, F.Q.; Chen, F.; Yang, L.-Z.; Jiang, T.; Qiu, G.-Z. Behavior of vanadium during reduction and smelting of vanadium titanomagnetite metallized pellets. *Trans. Nonferrous Met. Soc. China* **2020**, *30*, 1687–1696. [[CrossRef](#)]
11. Yang, M.Q.; Yang, J.Y. Vanadium extraction from steel slag: Generation, recycling and management. *Environ. Pollut.* **2024**, *343*, 123126. [[CrossRef](#)]
12. Li, H.Y.; Wang, K.; Hua, W.H.; Yang, Z.; Zhou, W.; Xie, B. Selective leaching of vanadium in calcification-roasted vanadium slag by ammonium carbonate. *Hydrometallurgy* **2016**, *160*, 18–25. [[CrossRef](#)]
13. Han, J.; Zhang, J.; Zhang, J.; Chen, X.; Zhang, L.; Tu, G. Recovery of Fe, V, and Ti in modified Ti-bearing blast furnace slag. *Trans. Nonferrous Met. Soc. China* **2022**, *32*, 333–344. [[CrossRef](#)]
14. Liu, S.G.; Ding, E.M.; Ning, P.; Xie, G.; Yang, N. Vanadium extraction from roasted vanadium-bearing steel slag via pressure acid leaching. *J. Environ. Chem. Eng.* **2021**, *9*, 105195. [[CrossRef](#)]
15. Wang, J.; Zhang, P.; Wang, S.D.; Yang, L.; Luo, J.H.; Shen, B. Mechanisms and kinetics of a new cleaner single cyclic roasting–leaching process for the extraction of vanadium from Linz–Donawitz converter slag using CaCO₃ and H₂SO₄. *Clean. Eng. Technol.* **2021**, *4*, 100204. [[CrossRef](#)]
16. Cheng, G.; Han, T.; Zhang, X.; Xue, X.; Yang, H.; Bai, R.; Zhang, W. A novel method of enhancing valuable element recovery for ultra-high-titanium magnetite. *J. Clean. Prod.* **2023**, *410*, 137184. [[CrossRef](#)]
17. Zhang, J.H.; Zhang, W.; Zhang, L.; Gu, S.Q. Mechanism of vanadium slag roasting with calcium oxide. *Int. J. Miner. Process.* **2015**, *138*, 20–29. [[CrossRef](#)]
18. Hu, P.C.; Zhang, Y.M.; Liu, H.; Liu, T.; Li, S.; Zhang, R.B.; Guo, Z.J. High efficient vanadium extraction from vanadium slag using an enhanced acid leaching-coprecipitation process. *Sep. Purif. Technol.* **2023**, *304*, 122319. [[CrossRef](#)]
19. Yin, R.T.; Chen, L.; Qing, Z.F.; Xiao, H.B.; Weng, D.S. A novel complexation method for separation and recovery of low valence vanadium, iron and chromium from sulfuric acid solution. *J. Clean. Prod.* **2022**, *373*, 133640. [[CrossRef](#)]
20. Yan, J.S.; Dou, Z.H.; Zhang, T.A. Preparation of vanadium by the magnesiothermic self-propagating reduction and process control. *Nanotechnol. Rev.* **2022**, *11*, 1237–1247.
21. Valerii, I.U.; Roman, D.K.; Andrei, O.K. Nanoporous high-temperature filters based on Ti-Al ceramic SHS materials. *Ceram. Int.* **2020**, *46*, 23180–23185.

22. Prokopets, A.D.; Bazhina, P.M.; Konstantinov, A.S.; Chizhikov, A.P.; Antipov, M.S.; Avdeeva, V.V. Structural features of layered composite material TiB₂/TiAl/Ti6Al4V obtained by unrestricted SHS-compression. *Mater. Lett.* **2021**, *300*, 130165. [[CrossRef](#)]
23. Nikitin, P.Y.; Matveev, A.E.; Zhukov, I.A. Energy-effective AlMgB₁₄ production by self-propagating high-temperature synthesis (SHS) using the chemical furnace as a source of heat energy. *Ceram. Int.* **2021**, *47*, 21698–21704. [[CrossRef](#)]
24. Fan, X.Z.; Huang, W.Z.; Zhou, X.; Zou, B.L. Preparation and characterization of NiAl-TiC-TiB₂ intermetallic matrix composite coatings by atmospheric plasma spraying of SHS powders. *Ceram. Int.* **2020**, *46*, 10512–10520. [[CrossRef](#)]
25. Chen, Z.Y. Development status and prospects of vanadium industrial in the world. *Chin. J. Rare Metal* **1991**, *2*, 128.
26. Song, Y.L.; Dou, Z.H.; Liu, Y.; Zhang, T.A. Study on the preparation process of TiAl alloy by self-propagating metallurgy. *J. Mater. Eng. Perform.* **2023**, *33*, 660–669. [[CrossRef](#)]
27. Yu, B.; Sun, Z.H.; Chen, H.J.; Tang, H.J.; Jing, H.; Du, G.C. Preparation and influence factors of FeV50 alloy based on gradient distribution of Al addition. *Chin. J. Rare Metal* **2017**, *41*, 1279–1284.
28. Xian, Y. Effects of Al content on phase transformation in FeV50 and its mechanism. *Iron Steel Vanadium Titan.* **2012**, *33*, 14.
29. Sun, Z.H. Analysis on new vanadium technologies and prospects of vanadium industry. *Iron Steel Vanadium Titan.* **2012**, *33*, 1.
30. Xian, Y.; Zhai, Q.J.; Sun, Z.H. Gradient smelting of ferrovanadium masteralloy by electro-aluminothermic process. *Chin. J. Rare Metal* **2016**, *40*, 850.
31. Li, L.; Ge, W.S.; Chen, Y. Study on Slag Corrosion of the Magnesia Lining during Ferrovanadium Smelting Process. *Adv. Mater. Res.* **2013**, *779*, 96–100. [[CrossRef](#)]
32. GB/T 40301-2021; Vanadium Trioxide. Chinese Standards Press: Beijing, China, 2021.
33. TB YB/T 5304-2017; Vanadium Pentoxide. Chinese Standards Press: Beijing, China, 2017.
34. GB/T 4139-2012; Ferrovanadium. Chinese Standards Press: Beijing, China, 2012.
35. QB-2021; Ingredients Standard and Operating Rules for Ferrovanadium. Pangang Group Vanadium & Titanium Resources Co., Ltd.: Panzhihua, China, 2021.
36. Yu, B.; Yuan, T.C.; Shi, J.J. Preparation of high-quality FeV50 alloy by an improved SHS-EAH multi-stage process. *Ceram. Int.* **2023**, *49*, 15114–15121. [[CrossRef](#)]
37. Jung, I.H.; Decterov, S.A.; Pelton, A.D. Critical thermodynamic evaluation and optimisation of the MgO–Al₂O₃, CaO–MgO–Al₂O₃, and MgO–Al₂O₃–SiO₂ systems. *J. Phase Equilib. Diffus.* **2004**, *25*, 329–345. [[CrossRef](#)]
38. Yu, B.; Yuan, T.C.; Xiao, D.H. Existing states of vanadium in slag during the preparation of FeV50 by aluminum thermal reduction. *Iron Steel Vanadium Titan.* **2019**, *40*, 24–29.
39. Xian, Y.; Zheng, H.X.; Zhai, Q.J.; Luo, Z.P. A two-dimensional structure map for prediction of the transition-metal Laves phases. *Comput. Mater. Sci.* **2016**, *125*, 1–7. [[CrossRef](#)]
40. Yu, B.; Zhou, H.; Sun, Z.H. Theoretical application and factors influencing casting settlement of FeV50 alloy. *Chin. J. Eng.* **2017**, *39*, 1822–1826.
41. Ye, M.F.; Yu, B.; Huang, Y.; Jing, H. Trend and control of P in FeV50 smelting process of large-scale tilting furnace. *Iron Steel Vanadium Titan.* **2022**, *43*, 36–41.
42. Wang, J.; Zhang, P.; Wang, S.D. Evaluation of a green-sustainable industrialized cleaner production for FeV50 and FeV80 alloys from vanadium slag by calcification roasting-ammonia on-line cycle. *J. Clean. Prod.* **2021**, *320*, 128896. [[CrossRef](#)]

Disclaimer/Publisher’s Note: The statements, opinions and data contained in all publications are solely those of the individual author(s) and contributor(s) and not of MDPI and/or the editor(s). MDPI and/or the editor(s) disclaim responsibility for any injury to people or property resulting from any ideas, methods, instructions or products referred to in the content.